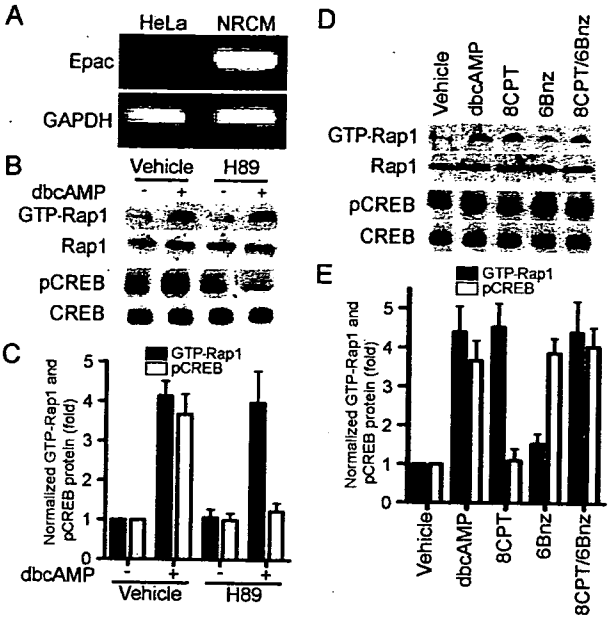

Figure 3. cAMP induces Epac-Rap1 signal as well as PKA signal in NRCMs. A, RT-PCR analysis shows the expression of Epac in NRCMs but not in HeLa cells (used as a negative control). GAPDH was shown as a positive control for RT-PCR. B, Serum-starved NRCMs were stimulated with 1 mmol/L dbcAMP in the absence or presence of H89 for 15 minutes. GTP-bound Rap1 were assessed by pull-down assay. Phosphorylation of CREB was analyzed by Western blot analysis using anti-CREB and anti-phospho-CREB (pCREB). A representative result of 3 independent experiments is shown. C, Data obtained from 4 independent experiments were analyzed quantitatively. Fold activation indicates the ratio of the poststimulation GTP-Rap1 and pCREB intensity of total Rap1 and CREB intensity to the prestimulation GTP-Rap1 and pCREB intensity of total Rap1 and CREB intensity. D, Serum-starved NRCMs were stimulated with either vehicle, 1 mmol/L dbcAMP, 1 mmol/L 8CPT, 1 mmol/L 6Bnz, or 1 mmol/L 8CPT and 1 mmol/L 6Bnz for 15 minutes. GTP-bound Rap1 and phosphorylation of CREB were assessed as described in B. E, Data obtained from 4 independent experiments were analyzed similarly to C.

endothelial–cadherins (VE-cadherins).[18,29] Thus, it is possible that cAMP enhances GJ neoformation by enhancing N-cadherin–mediated AJ formation preceding the GJ formation in NRCMs. To address this possibility, we investigated whether cAMP induces N-cadherin–mediated AJ formation in NRCMs. N-cadherin distribution at cell–cell contacts was enhanced by dbcAMP and 8CPT, whereas 6Bnz neither affected the distribution of N-cadherin nor enhanced the effect of 8CPT (Figure 5A).

To quantitatively analyze the localization of N-cadherin after drug treatment, we performed a biochemical N-cadherin translocation assay. Because N-cadherin is connected to actin cytoskeleton in maturated AJs, cadherin anchored to actin cytoskeleton can be detected in detergent-insoluble fractions of cell lysates. We found an increase in N-cadherin in Triton X-100–insoluble fraction when stimulated by dbcAMP and 8CPT (Figure 5B). However, 6Bnz did not change either basal- or 8CPT-increased levels of N-cadherin in the Triton X-100–insoluble fraction (Figure 5B and 5C). Collectively, these findings indicate that cAMP enhances AJ formation through Epac in NRCMs. We found no difference in N-cadherin expression in NRCMs stimulated with dbcAMP, 8CPT, or 6Bnz, or a combination of 8CPT and 6Bnz by immunoblotting (data not shown).

Rap1 Activation Is Essential for cAMP-Mediated Cx43 Redistribution and AJ Formation

We investigated the role of Rap1 in cAMP-induced Cx43 accumulation and AJ formation in NRCMs. To examine the effect of Rap1 on AJ and GJ formation, we inactivated Rap1 by adenovirus-expressing Rap1GAP1b, which specifically catalyzes the hydrolysis of GTP to GDP on Rap1.[30] Endogenous Rap1 activity was almost completely suppressed by the expression of increasing amount of Rap1GAP1b in NRCMs (Figure 6A). Moreover, overexpression of Rap1GAP1b inhibited cAMP-induced Rap1 activity without affecting cAMP-stimulated CREB phosphorylation (Figure 6B), confirming that Rap1GAP1b specifically blocks Epac-Rap1 pathway but not PKA-mediated signaling.

Inactivation of Rap1 blocked the cAMP-induced accumulation of Cx43 and N-cadherin at the cell–cell contacts (Figure 6C and 6D). dbcAMP-induced translocation of N-cadherin to cytoskeleton-anchored fraction was inhibited by inactivation of Rap1 but not by LacZ overexpression (Figure 6E and 6F). These results suggest that cAMP induces N-cadherin–based AJ assembly through an Epac-Rap1 signaling pathway, which may precede the accumulation of Cx43-based GJs.

PKA and Epac-Rap1 Signaling Cooperatively Enhances GJ Neoformation in NRCMs

Because we found that PKA alone is not sufficient for cAMP-enhanced GJ neoformation and that Epac-Rap1 signaling is involved in cAMP-induced accumulation of Cx43, we assessed the effect of PKA activation and Epac-Rap1 activation on gating function of GJs. 8CPT merely showed the weak enhancement of the intercellular connection, as revealed by microinjected dye transfer assay (Figure 7A). However, 8CPT significantly enhanced 6Bnz-mediated intercellular communication (Figure 7B). The effect of the combination of 8CPT and 6Bnz was comparable to that of dbcAMP. Given that 8CPT induces the Cx43 accumulation at the cell–cell contacts, cAMP potentiates functional GJ neoformation via a PKA-mediated enhanced gating function and Epac-Rap1 signal-mediated accumulation of Cx43 to cell–cell contacts.

Discussion

The function of GJs in the heart depends on the number of GJs between neighboring cells and the gating function of individual GJ at the cell–cell contacts. We investigated how cAMP induces Cx43 accumulation at cell–cell contacts and enhances gating function in NRCMs that were about to develop the mature cell–cell contacts. For the first time, we demonstrated the involvement of Epac-Rap1 signaling downstream of cAMP in GJ neoformation of cardiomyocytes. Although Cx43 accumulated at the cell–cell contacts on cAMP stimulation has been ascribed to PKA,[7] this study demonstrated that Epac-Rap1 signaling activated by cAMP is mainly responsible for the redistribution of Cx43 to cell–cell contacts.

The number of GJs was increased by Epac-Rap1 downstream of cAMP as indicated by the increase in Cx43-positive puncta at cell–cell contacts. However, there was no increase in the amount of Cx43 after cAMP treatment, indicating the importance of the redistribution of Cx43 rather than increase of Cx43 transcription on cAMP. How does Epac signaling induce the accumulation of Cx43 at cell–cell contacts?

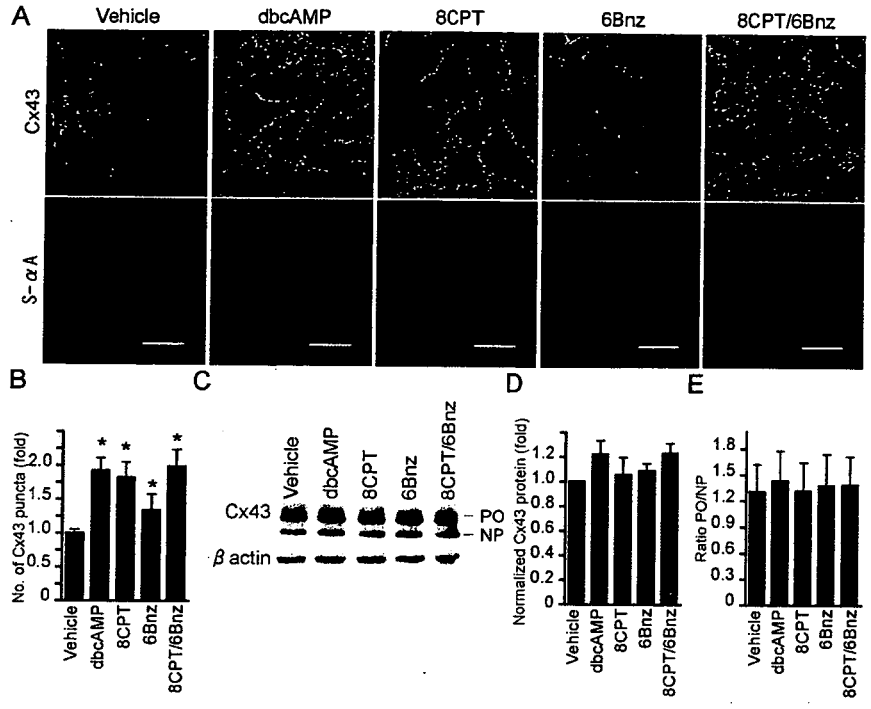

Figure 4. Activation of Epac signaling induces Cx43 accumulation at cell–cell contacts. A, NRCMs stimulated for 12 hours with drugs as indicated at the top were stained with anti-Cx43 and anti-S-αA as described in Figure 1A legend. Bar=20 μm. B, Cx43 accumulation was quantitatively analyzed in Figure 1B. Significant differences between vehicle-treated cells and all drug-treated cells was analyzed by one-way ANOVA with Scheffe's method (*$P<0.05$; n=6). C, NRCMs stimulated as indicated at the top were examined for Cx43 by Western blot analysis. Upper and lower bands correspond to phosphorylated (PO) and nonphosphorylated (NP) Cx43, respectively. D, Total Cx43 (phosphorylated and nonphosphorylated) expression of NRCMs treated for 12 hours with drugs as indicated at the bottom was quantitatively analyzed by three independent Western blot analyses for Cx43. The intensity of the drug-stimulated Cx43 normalized by β-catenin divided by that of vehicle-stimulated Cx43 was expressed as fold activation. E, The ratio is expressed by the intensity of phosphorylated Cx43 (PO) divided by that of nonphosphorylated Cx43 (NP).

Epac-Rap1 activation resulted in enhancement of AJ formation accompanied by GJ formation, as evidenced by increases in N-cadherin and Cx43 at the cell–cell contacts after dbcAMP stimulation (Figure 5). AJ formation constituted by N-cadherin is a prerequisite for GJ neoformation.[28,31] When adult myocytes are cultured, Cx43 is transported and accumulated at the plasma membrane, where N-cadherin accumulates on cell–cell contact.[26] Therefore, GJ formation depends on N-cadherin–based AJ maturation. We have shown previously that the Epac-Rap1 signal enhances the VE-cadherin–based cell–cell contacts in vascular endothelial cells.[18] In this study, we found that Epac activation resulted in the increased accumulation of N-cadherin at the intercellular junction of NRCMs. Thus, N-cadherin accumulation at the cell–cell contacts induced by the Epac-Rap1 signal may account for Cx43 accumulation in NRCMs by analogy to Epac-Rap1–triggered VE-cadherin accumulation in vascular endothelial cells.

The target of activated Rap1 for enhancement of cadherin-based AJ is still unclear. Rac belonging to Rho family GTPase and regulating actin cytoskeleton is suggested to function downstream of Rap1.[32] Therefore, Rac may increase the chances of cell contacts and induce cadherin engagement by extending membrane downstream of Rap1. Maturated N-cadherin on Epac activation, which is detected in the cytoskeleton-anchored fraction, may be accompanied by translocation of Cx43 through cadherin-associating β-catenin

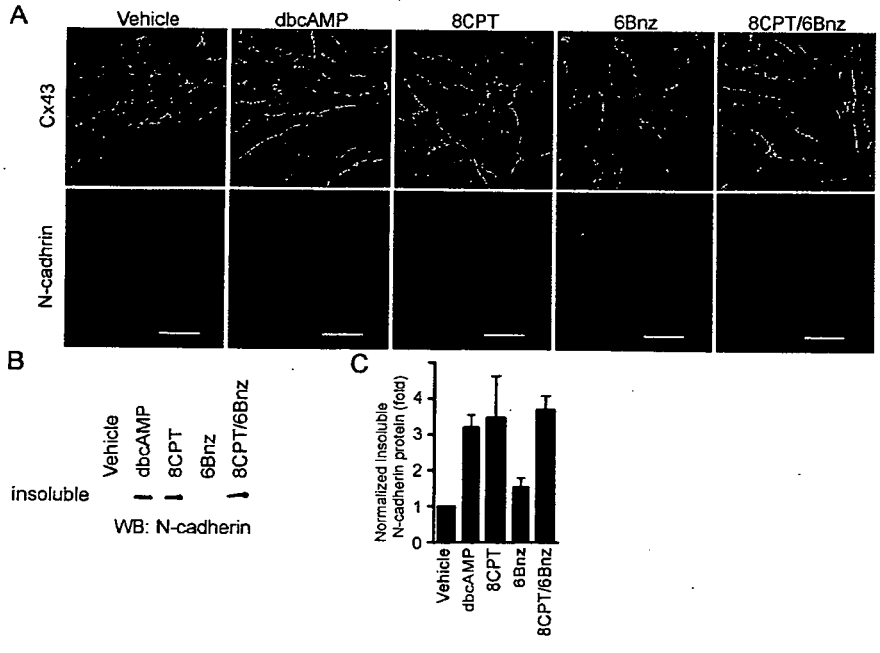

Figure 5. Activation of Epac induces AJ formation. A, NRCMs stimulated for 12 hours with drugs as indicated at the top were immunostained with anti-Cx43 (green) and anti-N-cadherin (red). Bar=20 μm. B, NRCMs stimulated as in A were fractionated with cytoskeleton stabilizing buffer. Triton X-100–insoluble fraction was subjected to SDS-PAGE followed by Western blot analysis (WB) with anti-N-cadherin. A representative result of three independent experiments is shown. C, The data obtained from three independent experiments of B was quantitatively analyzed. The result is indicated as fold increase calculated by dividing the amount of insoluble N-cadherin from the cells treated with the drug by that from the cells treated with vehicle.

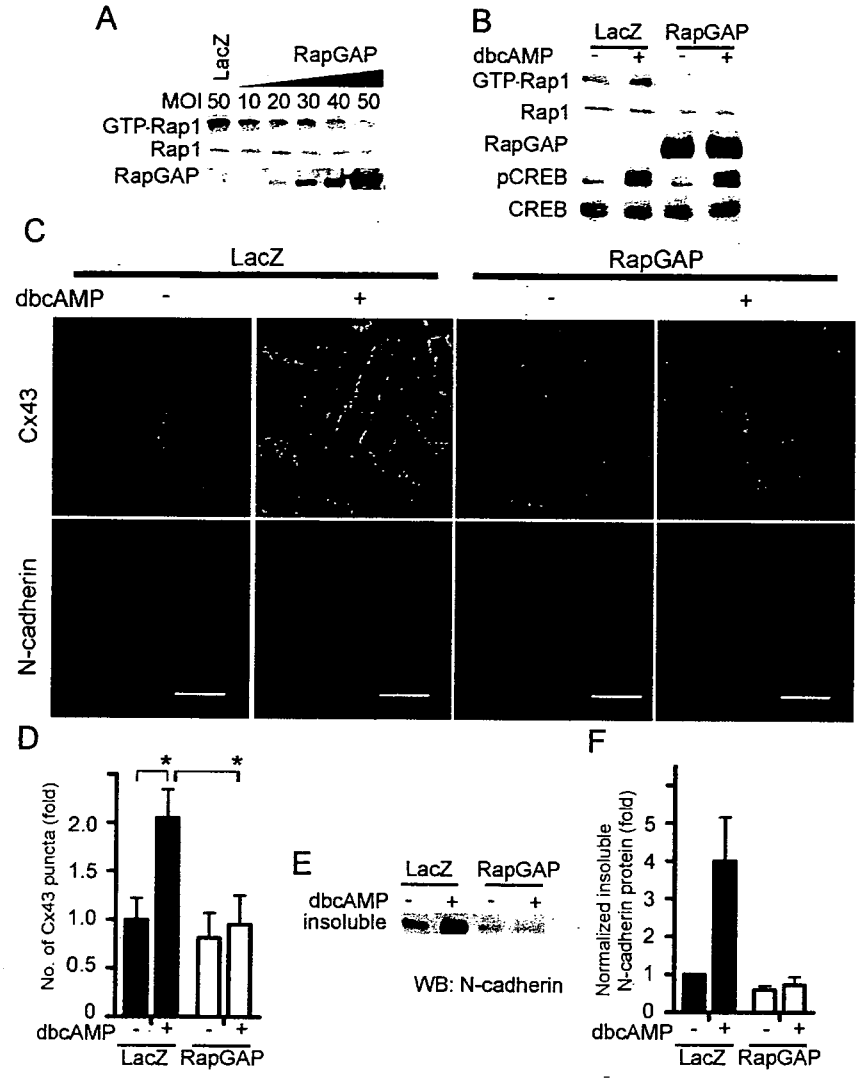

Figure 6. Rap1 activation is required for cAMP-induced Cx43 accumulation at the cell–cell contacts and AJ formation. A, Rap1 inactivation by Rap1GAP1b was verified by detecting GTP-Rap1 in NRCMs infected with different multiplicity of infection (MOI) of adenovirus-expressing Rap1GAP1b (Ad-RapGAP). An adenovirus-expressing LacZ (Ad-LacZ) at 50 MOI was used as a control. GTP-Rap1 was detected by pull-down assay. Rap1 and Rap1GAP1b (RapGAP) expression was examined by Western blot analysis using antibodies as indicated at the left. B, NRCMs infected with either Ad-LacZ or Ad-RapGAP at an MOI of 50 for 24 hours were stimulated with vehicle (−) or 1 mmol/L dbcAMP (+) for 15 minutes and analyzed for Rap1 and CREB activation. C, Localization of N-cadherin and Cx43 was examined similarly to Figure 5A in NRCMs infected with Ad-LacZ or Ad-RapGAP after stimulated with vehicle or 1 mmol/L dbcAMP for 12 hours. Bar=20 μm. D, The effect of inactivation of Rap1 on dbcAMP-induced accumulation of Cx43 was analyzed by two-way ANOVA with Scheffe's method, indicating that both factors, with/without dbcAMP and LacZ/RapGAP, are significant (*$P<0.05$; n=6). E, Translocation of N-cadherin was examined in NRCMs infected with Ad-LacZ or Ad-RapGAP after stimulation of dbcAMP. A representative of three independent results is shown. F, The three independent results from D were analyzed similarly to Figure 5C.

because Cx43 is capable of binding to β-catenin.[14] Because ZO-1 is recruited to AJs by binding to α-catenin and is also capable of binding to Cx43,[33] ZO-1 may participate in the accumulation of Cx43 during maturation of AJs.

Another factor affecting functional GJ neoformation in addition to the number of GJs is the gating function of individual GJs. PKA activation facilitates intercellular communication without accumulation of Cx43 at cell–cell contacts, concurring with previous reports underpinning that PKA and cAMP increases single channel conductance of the GJ,[34] although the characteristics of single GJ channel conductance evoked by PKA activation still remains elusive.[15]

We found a marked increase in dye transfer on PKA activation with a slightly increased accumulation of Cx43 at the cell–cell contacts (Figures 4 and 7). These results indicate that PKA mainly contributes to the functional neoformation of GJs by enhancing gating function of GJs. Phosphorylation of Cx43 on Ser residues is required for intercellular communication of GJs.[35] Because we found no significant increase in either total Cx43 or phosphorylated Cx43, PKA may indirectly modulate GJ conductance in addition to direct phosphorylation of Cx43 or may phosphorylate a critical Ser/Thr that was indistinguishable in the phosphorylated Cx43 band in our immunoblot for Cx43 (Figure 4C).

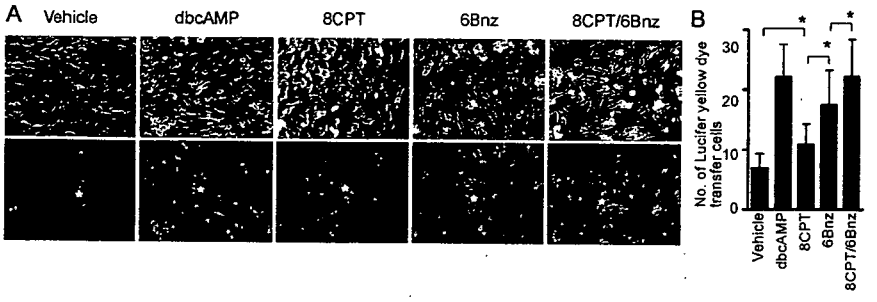

Figure 7. PKA signal and Epac-Rap1 signal cooperatively enhance intercellular communication through GJs. A, Intercellular communication was assessed by microinjected dye transfer assay using NRCMs stimulated with drugs as indicated at the top. B, Dye spread was quantitatively analyzed similarly to Figure 2F. Statistical significance between groups was evaluated by one-way ANOVA with Scheffe's method (*$P<0.05$; n=6).

The enhanced gating function of GJs is mainly ascribed to PKA, whereas the accumulation of Cx43 to cell–cell contacts is mainly attributable to Epac-Rap1 signal. Hence, Epac-Rap1 signal may accelerate the trafficking of Cx43 to the plasma membrane or inhibit the endocytosis of Cx43 from the plasma membrane. We did not quantify the translocation of Golgi fraction to cell–cell contacts on cAMP stimulation. Previously, GJ trafficking was dynamically monitored by green fluorescence protein–tagged Cx43.[36] Therefore, it will be of great interest to observe the Cx43 dynamics on 8CPT stimulation to directly elucidate Epac-Rap1 signaling.

In conclusion, we demonstrated that cAMP potentiates functional GJ neoformation by a PKA-dependent increase in intercellular communication and by an Epac-Rap1–dependent accumulation of Cx43 in NRCMs.

Acknowledgments

This work was supported in part by grants from the Ministry of Health, Labor, and Welfare Foundation of Japan; the Ministry of Education, Science, Sports, and Culture of Japan; the Promotion of Fundamental Studies in Health Science of the Organization for Pharmaceutical Safety and Research of Japan; the Japan Health Science Foundation; and Astellas Foundation for Research on Metabolic Disorders. We thank Michiyuki Matsuda and Akihiro Umezawa for their helpful input; Nobuo Shirahashi for statistical analysis; James T. Pearson and Michael E. Mendelsohn for critical reading; and Yuko Matsuura and Manami Sone for their technical assistance.

References

1. Yeager M. Structure of cardiac gap junction intercellular channels. *J Struct Biol.* 1998;121:231–245.
2. Sohl G, Willecke K. Gap junctions and the connexin protein family. *Cardiovasc Res.* 2004;62:228–232.
3. Vozzi C, Dupont E, Coppen SR, Yeh HI, Severs NJ. Chamber-related differences in connexin expression in the human heart. *J Mol Cell Cardiol.* 1999;31:991–1003.
4. Davis LM, Rodefeld ME, Green K, Beyer EC, Saffitz JE. Gap junction protein phenotypes of the human heart and conduction system. *J Cardiovasc Electrophysiol.* 1995;6:813–822.
5. Saffitz JE, Kleber AG. Effects of mechanical forces and mediators of hypertrophy on remodeling of gap junctions in the heart. *Circ Res.* 2004;94:585–591.
6. Gutstein DE, Morley GE, Fishman GI. Conditional gene targeting of connexin43: exploring the consequences of gap junction remodeling in the heart. *Cell Commun Adhes.* 2001;8:345–348.
7. Darrow BJ, Fast VG, Kleber AG, Beyer EC, Saffitz JE. Functional and structural assessment of intercellular communication. Increased conduction velocity and enhanced connexin expression in dibutyryl cAMP-treated cultured cardiac myocytes. *Circ Res.* 1996;79:174–183.
8. Paulson AF, Lampe PD, Meyer RA, TenBroek E, Atkinson MM, Walseth TF, Johnson RG. Cyclic AMP and LDL trigger a rapid enhancement in gap junction assembly through a stimulation of connexin trafficking. *J Cell Sci.* 2000;113:3037–3049.
9. Saffitz JE, Laing JG, Yamada KA. Connexin expression and turnover: implications for cardiac excitability. *Circ Res.* 2000;86:723–728.
10. Lampe PD, TenBroek EM, Burt JM, Kurata WE, Johnson RG, Lau AF. Phosphorylation of connexin43 on serine368 by protein kinase C regulates gap junctional communication. *J Cell Biol.* 2000;149:1503–1512.
11. TenBroek EM, Lampe PD, Solan JL, Reynhout JK, Johnson RG. Ser364 of connexin43 and the upregulation of gap junction assembly by cAMP. *J Cell Biol.* 2001;155:1307–1318.
12. Lin R, Warn-Cramer BJ, Kurata WE, Lau AF. v-Src phosphorylation of connexin 43 on Tyr247 and Tyr265 disrupts gap junctional communication. *J Cell Biol.* 2001;154:815–827.
13. Toyofuku T, Yabuki M, Otsu K, Kuzuya T, Hori M, Tada M. Direct association of the gap junction protein connexin-43 with ZO-1 in cardiac myocytes. *J Biol Chem.* 1998;273:12725–12731.
14. Ai Z, Fischer A, Spray DC, Brown AM, Fishman GI. Wnt-1 regulation of connexin43 in cardiac myocytes. *J Clin Invest.* 2000;105:161–171.
15. Schulz R, Heusch G. Connexin 43 and ischemic preconditioning. *Cardiovasc Res.* 2004;62:335–344.
16. Kawasaki H, Springett GM, Mochizuki N, Toki S, Nakaya M, Matsuda M, Housman DE, Graybiel AM. A family of cAMP-binding proteins that directly activate Rap1. *Science.* 1998;282:2275–2279.
17. de Rooij J, Zwartkruis FJ, Verheijen MH, Cool RH, Nijman SM, Wittinghofer A, Bos JL. Epac is a Rap1 guanine-nucleotide-exchange factor directly activated by cyclic AMP. *Nature.* 1998;396:474–477.
18. Fukuhara S, Sakurai A, Sano H, Yamagishi A, Somekawa S, Takakura N, Saito Y, Kangawa K, Mochizuki N. Cyclic AMP potentiates vascular endothelial cadherin-mediated cell-cell contact to enhance endothelial barrier function through an Epac-Rap1 signaling pathway. *Mol Cell Biol.* 2005;25:136–146.
19. Cullere X, Shaw SK, Andersson L, Hirahashi J, Luscinskas FW, Mayadas TN. Regulation of vascular endothelial barrier function by Epac, a cAMP-activated exchange factor for Rap GTPase. *Blood.* 2005;105:1950–1955.
20. Oyamada Y, Zhou W, Oyamada H, Takamatsu T, Oyamada M. Dominant-negative connexin43-EGFP inhibits calcium-transient synchronization of primary neonatal rat cardiomyocytes. *Exp Cell Res.* 2002;273:85–94.
21. Ogita H, Kunimoto S, Kamioka Y, Sawa H, Masuda M, Mochizuki N. EphA4-mediated Rho activation via Vsm-RhoGEF expressed specifically in vascular smooth muscle cells. *Circ Res.* 2003;93:23–31.
22. Doble BW, Chen Y, Bosc DG, Litchfield DW, Kardami E. Fibroblast growth factor-2 decreases metabolic coupling and stimulates phosphorylation as well as masking of connexin43 epitopes in cardiac myocytes. *Circ Res.* 1996;79:647–658.
23. Ohba Y, Ikuta K, Ogura A, Matsuda J, Mochizuki N, Nagashima K, Kurokawa K, Mayer BJ, Maki K, Miyazaki J, Matsuda M. Requirement for C3G-dependent Rap1 activation for cell adhesion and embryogenesis. *EMBO J.* 2001;20:3333–3341.
24. Christensen AE, Selheim F, de Rooij J, Dremier S, Schwede F, Dao KK, Martinez A, Maenhaut C, Bos JL, Genieser HG, Doskeland SO. cAMP analog mapping of Epac1 and cAMP kinase. Discriminating analogs demonstrate that Epac and cAMP kinase act synergistically to promote PC-12 cell neurite extension. *J Biol Chem.* 2003;278:35394–35402.
25. Enserink JM, Christensen AE, de Rooij J, van Triest M, Schwede F, Genieser HG, Doskeland SO, Blank JL, Bos JL. A novel Epac-specific cAMP analogue demonstrates independent regulation of Rap1 and ERK. *Nat Cell Biol.* 2002;4:901–906.
26. Hertig CM, Butz S, Koch S, Eppenberger-Eberhardt M, Kemler R, Eppenberger HM. N-cadherin in adult rat cardiomyocytes in culture. II. Spatio-temporal appearance of proteins involved in cell-cell contact and communication. Formation of two distinct N-cadherin/catenin complexes. *J Cell Sci.* 1996;109:11–20.
27. Kostetskii I, Li J, Xiong Y, Zhou R, Ferrari VA, Patel VV, Molkentin JD, Radice GL. Induced deletion of the N-cadherin gene in the heart leads to dissolution of the intercalated disc structure. *Circ Res.* 2005;96:346–354.
28. Kostin S, Hein S, Bauer EP, Schaper J. Spatiotemporal development and distribution of intercellular junctions in adult rat cardiomyocytes in culture. *Circ Res.* 1999;85:154–167.
29. Hogan C, Serpente N, Cogram P, Hosking CR, Bialucha CU, Feller SM, Braga VM, Birchmeier W, Fujita Y. Rap1 regulates the formation of E-cadherin-based cell-cell contacts. *Mol Cell Biol.* 2004;24:6690–6700.
30. Mochizuki N, Ohba Y, Kiyokawa E, Kurata T, Murakami T, Ozaki T, Kitabatake A, Nagashima K, Matsuda M. Activation of the ERK/MAPK pathway by an isoform of rap1GAP associated with G alpha(i). *Nature.* 1999;400:891–894.
31. Volk T, Geiger B. A 135-kDa membrane protein of intercellular adherens junctions. *EMBO J.* 1984;3:2249–2260.
32. Maillet M, Robert SJ, Cacquevel M, Gastineau M, Vivien D, Bertoglio J, Zugaza JL, Fischmeister R, Lezoualc'h F. Crosstalk between Rap1 and Rac regulates secretion of sAPPalpha. *Nat Cell Biol.* 2003;5:633–639.
33. Itoh M, Nagafuchi A, Moroi S, Tsukita S. Involvement of ZO-1 in cadherin-based cell adhesion through its direct binding to alpha catenin and actin filaments. *J Cell Biol.* 1997;138:181–192.
34. De Mello WC. Impaired regulation of cell communication by beta-adrenergic receptor activation in the failing heart. *Hypertension.* 1996;27:265–268.
35. Duncan JC, Fletcher WH. Alpha-1 connexin (connexin43) gap junctions and activities of cAMP-dependent protein kinase and protein kinase C in developing mouse heart. *Dev Dyn.* 2002;223:96–107.
36. Lauf U, Giepmans BN, Lopez P, Braconnot S, Chen SC, Falk MM. Dynamic trafficking and delivery of connexons to the plasma membrane and accretion to gap junctions in living cells. *Proc Natl Acad Sci U S A.* 2002;99:10446–10451.

Developmental stage-specific biphasic roles of Wnt/β-catenin signaling in cardiomyogenesis and hematopoiesis

Atsuhiko T. Naito*, Ichiro Shiojima*, Hiroshi Akazawa*, Kyoko Hidaka†, Takayuki Morisaki†, Akira Kikuchi‡, and Issei Komuro*§

*Department of Cardiovascular Science and Medicine, Chiba University Graduate School of Medicine, 1-8-1 Inohana, Chuo-ku, Chiba 260-8670, Japan; †Department of Bioscience, National Cardiovascular Center Research Institute, 5-7-1 Fujishirodai, Suita, Osaka 565-8565, Japan; and ‡Department of Biochemistry, Graduate School of Biomedical Sciences, Hiroshima University, 1-2-3 Kasumi, Minami-ku, Hiroshima 734-8551, Japan

Edited by Eric N. Olson, University of Texas Southwestern Medical Center, Dallas, TX, and approved October 23, 2006 (received for review July 10, 2006)

Although Wingless (Wg)/Wnt signaling has been implicated in heart development of multiple organisms, conflicting results have been reported regarding the role of Wnt/β-catenin pathway in cardiac myogenesis: Wg/armadillo signaling promotes heart development in *Drosophila*, whereas activation of Wnt/β-catenin signaling inhibits heart formation in avians and amphibians. Using an *in vitro* system of mouse ES cell differentiation into cardiomyocytes, we show here that Wnt/β-catenin signaling exhibits developmental stage-specific, biphasic, and antagonistic effects on cardiomyogenesis and hematopoiesis/vasculogenesis. Activation of the Wnt/β-catenin pathway in the early phase during embryoid body (EB) formation enhances ES cell differentiation into cardiomyocytes while suppressing the differentiation into hematopoietic and vascular cell lineages. In contrast, activation of Wnt/β-catenin signaling in the late phase after EB formation inhibits cardiomyocyte differentiation and enhances the expression of hematopoietic/vascular marker genes through suppression of bone morphogenetic protein signaling. Thus, Wnt/β-catenin signaling exhibits biphasic and antagonistic effects on cardiomyogenesis and hematopoiesis/vasculogenesis, depending on the stage of development.

cardiogenesis

Wnt genes encode secreted glycoproteins that play important roles in embryonic development, adult tissue homeostasis, and carcinogenesis (1, 2). During early embryogenesis, Wnt signaling is required for primitive streak formation and mesoderm induction (3, 4). Subsequently, Wnt signals regulate the patterning of anterior-posterior body plan: Wnt signaling is required for trunk/tail development and specification of posterior mesodermal fates, and Wnt inhibition in anterior ectoderm is required for head formation (3, 4). Regarding the role of Wnt signaling in heart formation and cardiomyocyte differentiation, there have been several contradictory reports, depending on the model organisms used. In avians and amphibians, the Wnt/β-catenin pathway inhibits cardiac development, and expression of Wnt inhibitors in the tissue adjacent to cardiac mesoderm is required for cardiogenesis (5–7). In contrast, the Wingless (Wg)/armadillo pathway (which corresponds to the Wnt/β-catenin pathway in vertebrates) promotes heart formation in *Drosophila* (8, 9), and Wnt/β-catenin signaling induces cardiomyocyte differentiation in a mouse embryonal carcinoma cell line P19CL6 (10, 11). Thus, Wnt/β-catenin signaling inhibits cardiogenesis in chick and *Xenopus*, whereas it enhances cardiogenesis in flies and in a mouse teratocarcinoma cell line.

To further explore the role of Wnt signaling during cardiac myogenesis, we used mouse ES cells as a model system for cardiomyocyte differentiation in mammals (12). We show here that activation of Wnt/β-catenin pathway in the early phase during embryoid body (EB) formation enhances ES cell differentiation into cardiomyocytes while suppressing hematopoietic and vascular cell marker gene expression. In contrast, activation of Wnt/β-catenin pathway in the late phase inhibits cardiomyocyte differentiation and enhances the expression of hematopoietic/vascular marker genes through the suppression of bone morphogenetic protein (BMP) signaling. Furthermore, initial enhancement followed by inhibition of Wnt/β-catenin signaling results in a marked increase in the efficiency of ES cell differentiation into cardiomyocytes. Thus, Wnt/β-catenin signaling exhibits developmental stage-specific, biphasic, and antagonistic effects on cardiogenesis and hematopoiesis/vasculogenesis, and appropriate modulation of Wnt signaling enables highly efficient cardiomyocyte differentiation of ES cells.

Results

Wnt Signaling Positively Regulates Cardiomyogenesis During Early Stage of ES Cell Differentiation. To induce ES cell differentiation into cardiomyocytes, EBs were formed by the hanging-drop method. Hanging-drop culture was started at day 0, and EBs were transferred to adhesion culture on day 3 (Fig. 1*A*). Under this experimental condition, spontaneous contraction was observed as small contracting foci in ≈80% of EBs at day 8 (Fig. 1*B*). To investigate the role of Wnt/β-catenin signaling in cardiomyocyte differentiation, we first analyzed the expression of Wnt ligands that activates Wnt/β-catenin pathway such as *Wnt1*, *Wnt3a*, and *Wnt8a*. During ES cell differentiation, *Wnt1* was expressed after day 4, *Wnt3a* on days 2 and 3, and *Wnt8a* from days 1 to 4 (Fig. 1*C*). Expression of early mesodermal markers (*Brachyury T*, *Goosecoid*) was detected from day 2, and cardiac lineage markers (*Csx/Nkx-2.5*, *Tbx-5*) were detectable from day 3 (Fig. 1*C*). Thus, initial commitment from immature mesodermal cells to a cardiac lineage occurs between days 2 and 3, when *Wnt3a* and *Wnt8a* genes are expressed. Next, we blocked Wnt/β-catenin signaling during this early stage of cardiomyocyte differentiation by extracellular Wnt inhibitors, Dickkopf-1 (Dkk-1; 500 ng/ml) and Frizzled-8/Fc chimeric protein (Fz8/Fc) (200 ng/ml), either alone or in combination. At these concentrations, Wnt3a (100 ng/ml)-induced activation of Wnt/β-catenin signaling in ht7 ES cells was completely suppressed as judged by a T cell factor-dependent reporter gene assay and the status of nuclear accumulation of β-catenin [supporting information (SI) Fig. 6]. When ES cells were treated with Dkk-1 in hanging

Author contributions: A.T.N., I.S., and I.K. designed research; A.T.N. performed research; H.A., K.H., T.M., and A.K. contributed new reagents/analytic tools; A.T.N. analyzed data; and A.T.N., I.S., and I.K. wrote the paper.

The authors declare no conflict of interest.

This article is a PNAS direct submission.

Abbreviations: BMP, bone morphogenetic protein; cTnT, cardiac troponin T; Dkk-1, Dickkopf-1; EB, embryoid body; Fz8/Fc, Frizzled-8/Fc chimeric protein; Wg, Wingless; DM, differentiation medium.

§To whom correspondence should be addressed. E-mail: komuro-tky@umin.ac.jp.

This article contains supporting information online at www.pnas.org/cgi/content/full/0605768103/DC1.

www.pnas.org/cgi/doi/10.1073/pnas.0605768103

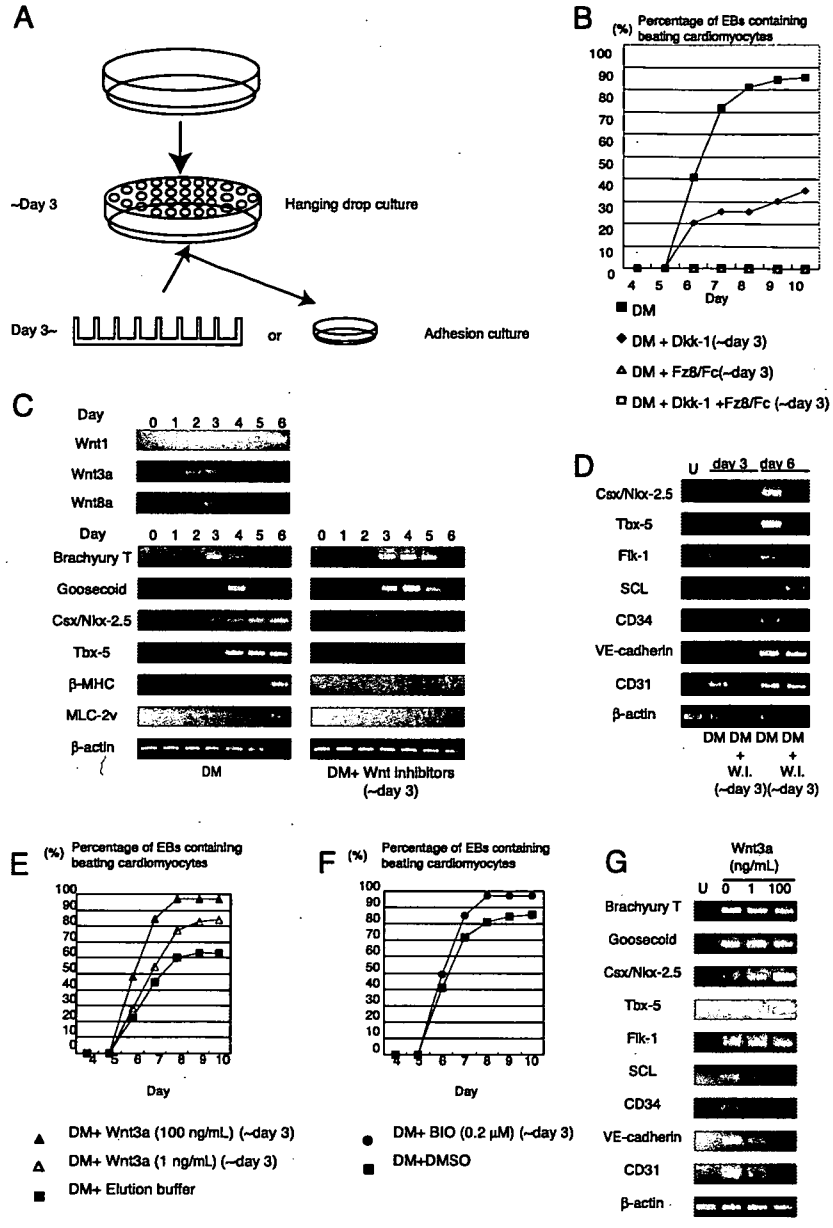

Fig. 1. Wnt/β-catenin signaling positively regulates cardiogenesis in the early stage of ES cell differentiation. (*A*) Protocol for cardiomyocyte differentiation of ES cells. (*B*) Number of EBs with beating foci. Wnt inhibitor treatment during EB formation suppressed differentiation into beating cardiomyocytes. (*C*) RT-PCR analysis of gene expression during differentiation of ES cells into cardiomyocytes. (*D*) Wnt inhibition blocked expression of cardiac markers and transiently down-regulated hematopoietic/vascular marker genes. Cells were cultured in the presence or absence of Wnt inhibitor during EB formation (until day 3). U, undifferentiated ES cells; W.I., Wnt inhibitors. (*E*) Number of EBs with beating foci. Wnt3a treatment during EB formation enhanced differentiation of ES cells into beating cardiomyocytes. (*F*) Number of EBs with beating foci. Treatment with BIO during EB formation enhanced differentiation of ES cells into beating cardiomyocytes. (*G*) RT-PCR analysis of cardiac, hematopoietic, and vascular cell lineage markers on day 3. U, undifferentiated ES cells.

drops from days 0 to 3, EBs were normally formed, but the number of EBs containing spontaneously beating foci was significantly suppressed (Fig. 1*B*). Moreover, when cells were treated with Fz8/Fc, or Dkk-1 plus Fz8/Fc, spontaneous contraction was never observed up to day 15 (Fig. 1*B* and data not shown). Although the precise reason for the differential effects of Dkk-1 vs. Fz8/Fc is not known, it may be due to slightly more efficient suppression of Wnt/β-catenin signaling by Fz8/Fc than that by Dkk-1 (SI Fig. 6*A*). Alternatively, β-catenin-independent, noncanonical Wnt signaling that is blocked by Fz8/Fc but not by Dkk-1 may partially contribute to Wnt-mediated cardiogenesis at this stage. Expression of earliest cardiac marker genes *Csx/Nkx-2.5* and *Tbx-5* was completely abolished by Wnt inhibitor treatment, whereas that of mesodermal marker genes *Brachyury* and *Goosecoid* was not affected by Wnt inhibition (Fig. 1 *C* and *D*). Thus, it is presumed that the commitment of mesodermal cells into a cardiomyocyte lineage requires higher levels of Wnt/β-catenin signaling than those required for specification of mesodermal cells. We also investigated whether differentiation into other mesoderm-derived cell lineages is affected by Wnt inhibition. Expression of early hematopoietic markers (*SCL* and *CD34*) and endothelial cell markers (*CD31* and *VE-cadherin*) was transiently down-regulated at day 3 but was not

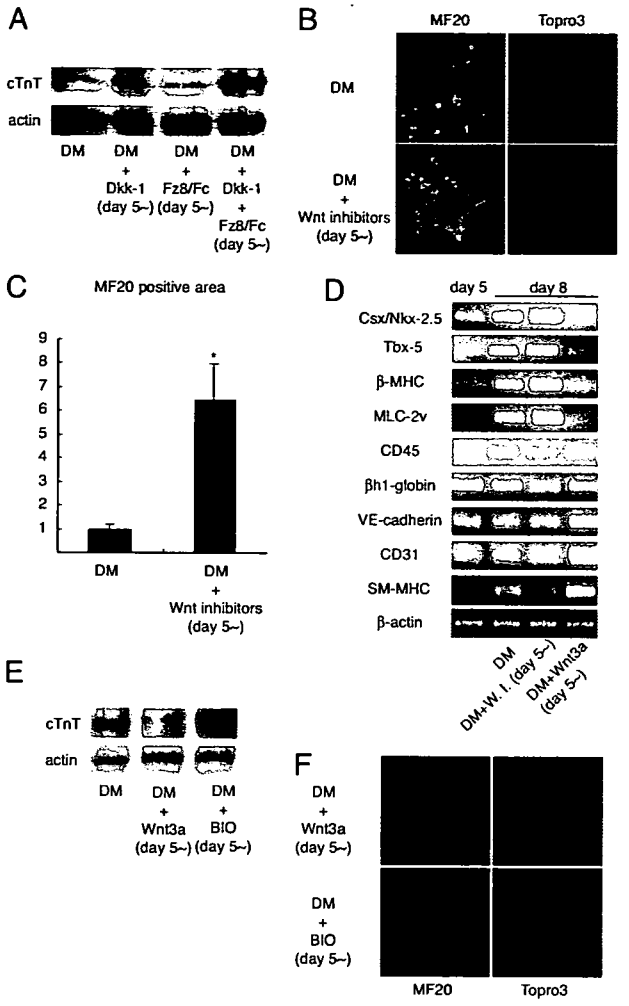

Fig. 2. Wnt/β-catenin signaling negatively regulates cardiogenesis in the late stage of ES cell differentiation. (*A*) Western blot analysis for cTnT on day 10. EBs were cultured in DM or DM containing the indicated Wnt inhibitors from day 5. Wnt inhibitor treatment after day 5 increased cTnT expression. (*B*) MF20 and Topro staining on day 10. (Magnification: ×100.) (*C*) Morphometry for the expression of sarcomeric MHC in each EB. *, $P < 0.01$ vs. control. (*D*) RT-PCR analysis of cardiac, hematopoietic, and vascular marker genes. EBs were cultured in DM or DM containing Wnt inhibitors (DM + W.I.) or Wnt3a protein (DM + Wnt3a) from day 5. W.I., Wnt inhibitors. (*E*) Western blot analysis for cTnT on day 10. EBs were cultured in DM or DM containing Wnt3a (DM + Wnt3a) or BIO (DM + BIO) from day 5. Wnt3a treatment in the late stage of ES cell differentiation blocks further differentiation into mature cardiomyocytes. (*F*) MF20 and Topro staining on day 10. (Magnification: ×100.)

altered at day 6. Expression of *Flk-1*, a marker of hemangioblasts as well as other mesodermal progenitors (13), was not affected by Wnt inhibition (Fig. 1*D*). Thus, inhibition of Wnt/β-catenin signaling transiently attenuates differentiation of ES cells into a hematopoietic or an endothelial cell lineage. Other mesoderm-derived cell markers such as *MyoD* (a marker of skeletal muscle) or *Runx2* (a marker of bone and cartilage) were not expressed at these time points (data not shown). Taken together, Wnt signaling in the early phase of ES cell differentiation is required for commitment of mesodermal cells into a cardiomyocyte lineage.

To further examine the role of Wnt/β-catenin signaling in the commitment of mesodermal cells into cardiomyocytes, we treated ES cells with purified Wnt3a protein during the early stage of ES cell differentiation. When Wnt3a was added from days 0 to 3, the relative number of beating EBs was increased in a dose-dependent manner (Fig. 1*E*). Slightly lower percentage of spontaneous beating in control EBs as compared with that shown in Fig. 1*B* is presumably due to the mild inhibitory effect of Wnt3a elution buffer on cardiomyocyte differentiation (Fig. 1 *B* and *E*). This effect of Wnt3a to promote cardiogenesis was mimicked by the addition of glycogen synthase kinase-3β inhibitor BIO (0.2 μM) from days 0 to 3, suggesting that β-catenin-dependent canonical Wnt signaling is responsible for this positive effect of Wnt3a on cardiomyocyte differentiation (Fig. 1*F*). We also examined the expression of cardiac, hematopoietic, and endothelial cell lineage markers in response to Wnt3a treatment at day 3. Addition of Wnt3a from days 0 to 3 dramatically increased the expression of *Csx/Nkx-2.5* and *Tbx-5*, whereas the expression of *SCL*, *CD34*, *VE-cadherin*, and *CD31* was decreased in a dose-dependent manner (Fig. 1*G* and SI Fig. 7). We also performed FACS analysis of hcgp7, a clonal derivative of ht7 ES cells in which GFP cDNA is knocked in at the Csx/Nkx2.5 locus (14). In response to Wnt3a treatment, there was a significant increase in the number of cells in a cardiac lineage (GFP positive) as well as a significant decrease in the number of cells in a hematopoietic (CD34 positive) or an endothelial cell (CD31 positive) lineage at day 3 of differentiation (SI Table 1). Thus, increased level of Wnt/β-catenin signaling during EB formation further enhances differentiation into cardiomyocytes and simultaneously inhibits differentiation of ES cells into hematopoietic and endothelial cell lineages.

Wnt Signaling Negatively Regulates Cardiomyogenesis During the Late Stage of ES Cell Differentiation. We next examined the role of Wnt/β-catenin signaling during later stage of cardiomyocyte differentiation, when cells are already committed to a cardiac lineage and start to express contractile protein genes. In our experimental condition, the expression of contractile protein genes such as *β-myosin heavy chain* (*β-MHC*) and *myosin light chain 2v* (*MLC-2v*) was first observed at around day 5 (Fig. 1*C*). Thus, Wnt inhibitor treatment was started at day 5, and late-stage cardiomyocyte differentiation was evaluated by Western blot analysis of cardiac troponin T (cTnT) on day 10. In contrast to the inhibitory effects of Wnt inhibitors on early-stage cardiomyocyte differentiation, late-stage cardiomyocyte differentiation was strongly promoted by Dkk-1 and only marginally by Fz8/Fc, and a combination of these two inhibitors synergistically enhanced this process (Fig. 2*A*). This effect is consistent with previous observations showing that Dkk-1 induces ectopic cardiogenesis in noncardiac mesoderm more efficiently than soluble frizzed receptor protein family of Wnt inhibitor such as Frzb (6). In addition, treatment with a combination of Wnt inhibitors (Dkk-1 plus Fz8/Fc) from day 5 increased the area of mature cardiomyocytes stained with MF20 (a monoclonal antibody against sarcomeric MHC) by 6-fold compared with control EBs on day 10 (Fig. 2 *B* and *C*). RT-PCR analysis revealed that treatment with Wnt inhibitors increased the expression of mature cardiac marker genes while the expression levels of mature hematopoietic (*CD45* and *βh1-globin*) or endothelial cell markers were decreased (Fig. 2*D* and SI Fig. 8). *Smooth muscle myosin heavy chain* (*SM-MHC*) gene, a marker of smooth muscle cells, was expressed from day 5 during ES cell differentiation (data not shown), and its expression was also decreased by Wnt inhibitor treatment (Fig. 2*D* and SI Fig. 8). Next, we activated Wnt/β-catenin signaling by treating EBs with Wnt3a or BIO beginning from day 5 of differentiation. In contrast to the effects of Wnt activation on early-stage cardiomyocyte differentiation, activation of Wnt/β-catenin signaling at this later stage completely suppressed the expression of cTnT (Fig. 2*E*) and abolished the appearance of spontaneously contracting EBs or MF20-positive cardiomyocytes on day 10 (Fig. 2*F*). The expression of cardiac marker genes was dramatically down-regulated, whereas that of hematopoietic, endothelial, or smooth muscle cell markers was up-regulated by Wnt3a treatment (Fig. 2*D* and SI Fig. 8). Collectively, these observations indicate that Wnt/

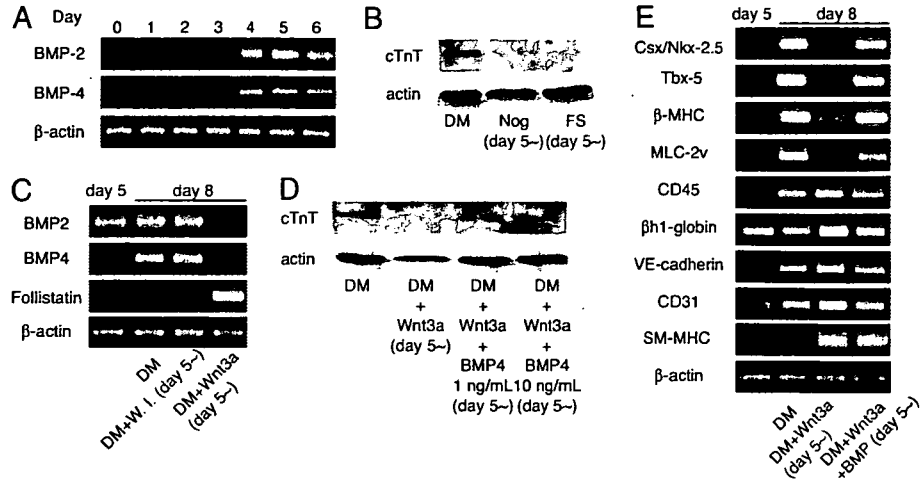

Fig. 3. Wnt inhibits cardiomyocyte differentiation in the late phase by suppressing BMP signaling. (*A*) RT-PCR analysis of BMP2/4 expression. (*B*) Western blot analysis for cTnT on day 10. EBs were cultured in DM or DM containing noggin (Nog) or follistatin (FS) from day 5. Inhibition of BMP signaling during the late phase suppresses cardiomyocyte differentiation. (*C*) RT-PCR analysis of BMP2/4 and Follistatin expression. EBs were cultured in DM or DM containing Wnt inhibitors (DM + Wnt inhibitors) or Wnt3a protein (DM + Wnt3a) from day 5. W.I., Wnt inhibitors. (*D*) Western blot analysis for cTnT on day 10. EBs were cultured in DM or DM containing Wnt3a (DM + Wnt3a) or Wnt3a plus BMP4 protein (DM + Wnt3a + BMP4) from day 5. Inhibition of cardiomyocyte differentiation by Wnt3a was rescued by BMP treatment. (*E*) RT-PCR analysis of cardiac, hematopoietic, and vascular marker genes. EBs were cultured in DM or DM containing Wnt3a (DM + Wnt3a) or Wnt3a plus BMP4 protein (DM + Wnt3a + BMP4) from day 5.

β-catenin signaling, when activated after cells are committed to cardiomyocytes, negatively regulates cardiomyocyte differentiation, and that inhibition of Wnt signaling at this stage enhances cardiomyocyte differentiation.

Activation of Wnt Signaling During the Late Stage Attenuates Cardiomyocyte Differentiation by Suppressing BMP Signaling. To further investigate the molecular mechanisms by which Wnt/β-catenin signaling shows such biphasic effects on cardiomyocyte differentiation, we investigated whether other signaling pathways that play an important role during cardiogenesis are affected by Wnt/β-catenin signaling. The BMP family of humoral factors positively regulate cardiogenesis in *Drosophila* (15), chick (16), *Xenopus* (17), mouse (18), and P19CL6 cells (19). Among the BMP family members, BMP2/4 are implicated in cardiogenesis (16) and are expressed predominantly during the late stage of ES cell differentiation into cardiomyocytes (Fig. 3*A*). Expression of BMP2/4 during this stage is indispensable for cardiomyocyte differentiation, because the addition of a BMP inhibitor such as noggin (100 ng/ml) or follistatin (100 ng/ml) during the later stage of ES cell differentiation decreased the expression of cTnT (Fig. 3*B*). Interestingly, activation of Wnt/β-catenin signaling during the late stage of ES cell differentiation suppressed the expression of BMP2/4 and induced the expression of follistatin (Fig. 3*C*), suggesting that the negative effect of Wnt signaling on cardiomyocyte differentiation in the late phase is mediated by inhibition of BMP pathway. To test this hypothesis, we treated EBs with a combination of Wnt3a and BMP4. Addition of BMP4 protein (1 and 10 ng/ml) rescued the Wnt3a-mediated inhibition of cardiomyocyte differentiation (Fig. 3*D*) and normalized the expression pattern of cardiac, hematopoietic, and vascular cell marker genes (Fig. 3*E*). In collection, these observations indicate that the antagonistic effects of Wnt/β-catenin signaling on cardiogenesis and hematopoiesis/vasculogenesis in the late phase of ES cell differentiation are in part mediated by Wnt-induced inhibition of BMP signaling.

Modulation of Wnt Signaling Enables Efficient Induction of Cardiomyocytes from ES Cells. Finally, we tested the hypothesis that activation of Wnt/β-catenin signaling in the early phase (from days 0 to 3) followed by Wnt inhibition in the late phase (from day 5 and afterward) might further enhance cardiomyocyte differentiation of ES cells. Activation of Wnt signaling in the early phase or inhibition of Wnt signaling in the late phase each increased MF20-positive area ≈6-fold (Fig. 4 *A* and *B*). Wnt activation in the early phase followed by Wnt inhibition in the late phase further increased MF20-positive area per single EB up to 13-fold (Fig. 4 *A* and *B*). This increase in MF20-positive area was associated with increased expression of *Csx/Nkx2.5* and *Tbx5* and decreased expression of *SCL* and *βh1-globin* (Fig. 4*C*; SI Fig. 9). Enhanced cardiomyocyte differentiation and diminished hematopoietic differentiation was also confirmed by Western blot analysis of cTnT expression and FACS analysis of hcgp7 cells on day 10 of differentiation (Fig. 4*D*; SI Table 2). Thus, appropriate modulation of Wnt signaling enables highly efficient induction of ES cell differentiation into cardiomyocytes.

Discussion

Although previous studies have implicated Wg/Wnt signaling in cardiac development, there exist some controversies regarding the roles of Wg/Wnt in cardiogenesis. In *Drosophila*, elimination of Wg function for a short time period after gastrulation results in loss of heart formation, and overexpression of Dishevelled leads to increased number of heart precursor cells (8, 9). Likewise, Wnt/β-catenin signals are essential for *in vitro* cardiomyocyte differentiation of mouse P19CL6 cells, a teratocarcinoma-derived pluripotent cell line (10, 11). However, in chick embryos at stage 5–6, Wnt3 and Wnt8 are expressed in the posterior part of the embryo (primitive streak and adjacent ectodermal cells) and block cardiogenesis in this region (5). At stage 8–9, Wnt1 and Wnt3 are expressed in the neural tube, and this Wnt signal from neural tube blocks cardiogenesis in the anterior paraxial mesoderm (7). In *Xenopus* embryos, forced expression of Wnt ligands in dorsal mesoderm (which normally gives rise to the heart) inhibits cardiac marker gene expression (6). Taken together, the Wnt/β-catenin pathway promotes cardiogenesis in *Drosophila* and mouse P19CL6 cells, whereas it blocks heart formation in chick and *Xenopus*.

Based on our present study, one possible explanation for this apparent discrepancy is that Wnt/β-catenin signaling has biphasic

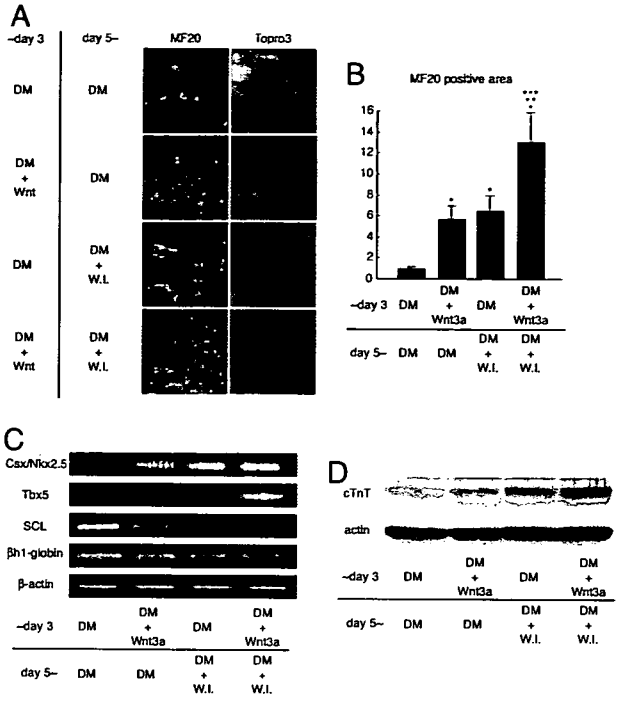

Fig. 4. Activation of Wnt signaling in the early stage followed by Wnt inhibition in the late stage leads to highly efficient differentiation of ES cells into cardiomyocytes. (*A*) MF20 and Topro staining on day 10. (Magnification: ×100.) (*B*) Morphometry for the expression of sarcomeric MHC in each EB. *, $P < 0.05$ vs. "DM>DM" protocol. **, $P < 0.05$ vs. "DM + Wnt3a>DM" protocol. ***, $P < 0.05$ vs. "DM>DM + Wnt inhibitor" protocol. (*C*) RT-PCR analysis of cardiac and hematopoietic markers. (*D*) Western blot analysis of cTnT expression on day 10.

effects on cardiogenesis depending on the stage of differentiation. According to this model, Wnt signaling promotes commitment of mesodermal cells into a cardiac lineage in the early phase of cardiogenesis while it inhibits proliferation and/or maturation of committed cardiomyocytes in the late phase of cardiac development. In *Drosophila*, temporal requirement of Wg for heart formation is restricted to a short time period after gastrulation, which is much earlier than the time point when the expression of a *Csx/Nkx-2.5*-related gene *tinman* becomes restricted to dorsal cardiac mesoderm (8). During P19CL6 cell differentiation into cardiomyocytes, expression of *Wnt3a* and *Wnt8a* genes is observed earlier than that of early cardiac markers, and inhibition of Wnt signaling in the early stage results in the suppression of cardiac marker gene expression without affecting mesodermal marker gene expression (10, 11). These observations support the notion that Wnt/β-catenin signaling promotes commitment of mesodermal cells into a cardiomyocyte lineage. In chick and *Xenopus*, negative effects of Wnt signals on cardiogenesis are observed in precardiac mesoderm, where cells are supposed to be already committed to a cardiomyocyte lineage. In support of this hypothesis, it was reported that hemangioblast commitment is already initiated during gastrulation in the primitive streak (20). By analogy, the cell fate decision into a cardiac lineage may occur during gastrulation in the primitive streak, where a high concentration of local Wnt ligands promotes this process, and then committed cells migrate to heart forming region by gastrulation movements where they are exposed to Wnt inhibitors to form mature cardiomyocytes.

Wnt/β-catenin signaling is required for primitive streak formation and mesoderm induction *in vivo* (3, 4) and the generation of ES cell-derived mesoderm *in vitro* (21). Thus, one might argue that the positive effects of Wnts on cardiogenesis in the early stage of differentiation reflect the mesoderm-inducing activity of Wnt signaling. However, we favor the model in which additional Wnt activity is required to induce commitment of immature mesodermal cells into a cardiac lineage, because Wnt inhibitor treatment in the early phase (from days 0 to 3) did not attenuate the expression of mesodermal markers while completely abolishing early cardiac marker gene expression in our experimental condition. The discrepancy between the present work and a previous study (21) may be due to a difference in the ES cell differentiation protocol. Alternatively, the concentration of Wnt inhibitors used in our study might be subthreshold level to completely block mesodermal differentiation (Fig. 1*C*). During gastrulation, heart progenitor cells leave the primitive streak and move anterolaterally to reside at the anterior end of the mesoderm, making the heart the most anterior mesoderm-derived organ to develop in vertebrates. In this regard, the requirement of Wnt inhibitors for cardiogenesis in the later stage of ES cell differentiation may reflect the regulation of anterior-posterior body plan by Wnt signaling.

Another important point is that Wnt signal has antagonistic effects on cardiogenesis vs. hematopoiesis/vasculogenesis in both the early and late stages of differentiation. Wnt/β-catenin signaling was initially proposed to increase hematopoietic stem cell (HSC) self-renewal and enhance their ability to reconstitute the hematopoietic system of lethally irradiated animals (2). On the other hand, constitutive activation of Wnt/β-catenin signaling in hematopoietic system results in differentiation block of HSCs and widespread hematopoietic abnormalities (22, 23), together suggesting that fine-tuned control of Wnt signaling is required for HSC self renewal and differentiation. This notion is consistent with our observations that both activation and inhibition of Wnt signaling in the early phase of ES cell differentiation result in down-regulation of hematopoietic marker genes. Regarding the antagonistic effects of Wnt signaling on cardiogenesis and hematopoiesis in the late phase of ES cell differentiation, similar effects of Wnt signaling on cardiogenesis vs. hematopoiesis have been reported in chick and frog embryos: Wnt inhibition in posterior mesoderm (which normally gives rise to blood) leads to induction of cardiac markers and simultaneous inhibition of hematopoietic marker gene expression (5), and forced expression of Wnt ligands in precardiac mesoderm leads to inhibition of cardiogenesis and ectopic expression of hematopoietic markers (5, 6).

We have also shown that Wnt-induced inhibition of cardiogenesis and promotion of hematopoiesis/vasculogenesis in the late phase are in part mediated by Wnt-induced inhibition of BMP signaling. This notion is consistent with a recent report showing that inhibition

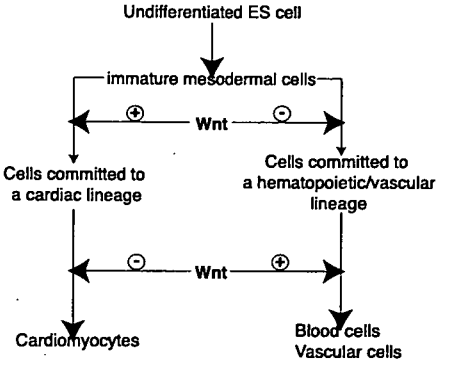

Fig. 5. Wnt signals exhibit developmental stage-specific, biphasic, and antagonistic effects on cardiogenesis and hematopoiesis. In the early stage of development, Wnt signals promote cardiogenesis and inhibit hematopoiesis, whereas in the late stage of development, Wnt signals inhibit cardiomyocyte differentiation and promote blood cell differentiation.

of BMP signaling enhances hematovascular development in lateral mesoderm in zebrafish (24). Wnt-induced BMP inhibition is also reported by previous studies showing that Wnt/β-catenin signaling attenuates the expression of BMP4 during neurogenesis (25) and promotes the expression of follistatin in mouse embryonal carcinoma cells (26). However, it should be noted that Wnt-mediated inhibition of BMP signal is context-dependent, because Wnt3a induces the expression of BMP4 in a different cell type (27).

Collectively, our present study indicates that Wnt signals have developmental stage-specific, biphasic, and antagonistic effects on both cardiogenesis and hematopoiesis/vasculogenesis (Fig. 5) and provides important clues to the dissection of cardiogenic signaling pathways during embryogenesis. It also demonstrates that differentiating ES cells represent a useful model system for the dissection of complex regulatory networks that control organogenesis during embryonic development.

Materials and Methods

Reagents. Recombinant mouse Dkk-1, mouse Fz8/Fc, mouse noggin/Fc chimera, mouse Follistatin 288, and human BMP4 proteins were purchased from R&D (Minneapolis, MN). The glycogen synthase kinase-3β inhibitor, BIO, was from Calbiochem (La Jolla, CA). Wnt3a protein was purified as described (28). Elution buffer for Wnt3a protein contains 1% CHAPS and 30 mM imidazole. Same amount of elution buffer was added to the culture medium when using purified Wnt3a protein.

ES Cell Culture and Differentiation Protocol. The 129/Ola-derived ht7 ES cells (29) and hcgp7 ES cells (14) were used in this study. ES cells were maintained on gelatin-coated dishes without feeder cells by using growth medium containing 2,000 units/ml leukemia inhibitory factor (ESGRO; Chemicon, Hampshire, U.K.). For differentiation, 500 ES cells in 30-μl aliquots of (DM; growth medium without leukemia inhibitory factor) were cultured in hanging drop for 3 days. On the third day, the resultant individual EBs were transferred to gelatin-coated 48-well culture plates or a 35-mm dish. To evaluate the differentiation efficiency of ES cells, 48-well plates were monitored every day under a microscope to detect the appearance of spontaneously contracting cardiomyocytes, and the percentage of the EBs that exhibited spontaneous contraction was calculated as differentiation efficiency. More than 200 wells were observed to calculate differentiation efficiency at each time point. The medium was changed every other day. The day when hanging drop culture was started was defined as day 0.

RT-PCR and Quantitative Real-Time PCR. Total RNA extraction and DNase treatment were performed by using the SV total RNA isolation Kit (Promega, Madison, WI). RT-PCR was performed as described (10). Every PCR condition was confirmed to be within the semiquantitative range for specific genes and primer pairs. Expression of β-actin was used as internal control. Real-time PCR was performed by using the LightCycler (Roche, Indianapolis, IN) according to the manufacturer's instructions. Individual PCR products were analyzed by melting-point analysis. β-Actin was used as an internal control to normalize for RNA amounts. Relative levels of gene expression were normalized to the β-actin gene by using the comparative Ct method according to the manufacturer's instructions. Primer sequences for both semiquantitative and quantitative PCR are available upon request.

Western Blotting. Western blotting was performed as described (10). Signal was detected by using ECL detection kit (Amersham Biosciences, Piscataway, NJ).

Immunohistochemistry. Immunohistochemistry was performed as described (30). Mouse monoclonal antisarcomeric myosin heavy chain (MF20; Developmental Studies Hybridoma Bank maintained at the University of Iowa, Department of Biological Sciences, Iowa City, IA) was used as a primary antibody, and FITC-conjugated secondary antibody was applied to visualize expression of specific proteins. Before mounting, nuclei were stained with Topro3 (Molecular Probes, Eugene, OR). Images of samples were taken by laser confocal microscopy (Radiance 2000; Bio-Rad Laboratories, Hercules, CA). For morphometric analysis for the expression of sarcomeric myosin heavy chain stained with MF20, all aspects of cell processing, immunostaining, and imaging were rigorously standardized. To exclude the possibility that variations in immunostaining on different samples affected the morphometric data, all samples in the same data set were immunostained and analyzed at the same time. Digital images were obtained from at least four EBs using the ×10 objective lens. Four images from at least three independent immunostained samples were used for morphometric analysis. The MF20-positive area was calculated as fold increase to that of control EB induced to differentiate into cardiomyocytes with no extra treatment.

FACS Analysis. FACS was performed by using EPICS ALTRA (Beckman Coulter, Fullerton, CA). Cells were dissociated by using 0.05% trypsin (Invitrogen) in PBS and stained with phycoerythrin (PE)-conjugated anti-CD31, -CD34, or -CD45 (all from e-bioscience, San Diego, CA) for 30 min on ice and washed twice with PBS supplemented with 2% FBS. PE and GFP were detected by using a 488-nm argon laser.

Statistical Analysis. Data are expressed as mean ± standard deviation. The significance of differences among means was evaluated by using ANOVA, followed by Fisher's probable least-squares difference test for multiple comparisons. Significant differences were defined as $P < 0.05$.

We thank Hitoshi Niwa (Osaka University, Osaka, Japan) for the ht7 ES cells. This work was supported in part by grants from the Japanese Ministry of Education, Science, Sports, and Culture; the Japan Health Sciences Foundation; Health and Labor Sciences; and the Japan Medical Association (to I.K.); and by a Japan Heart Foundation Young Investigator's Research Grant (to A.T.N.).

1. Logan CY, Nusse R (2004) *Annu Rev Cell Dev Biol* 20:781–810.
2. Reya T, Clevers H (2005) *Nature* 434:843–850.
3. Yamaguchi TP (2001) *Curr Biol* 11:R713–R724.
4. Kimelman D (2006) *Nat Rev Genet* 7:360–372.
5. Marvin MJ, Di Rocco G, Gardiner A, Bush SM, Lassar AB (2001) *Genes Dev* 15:316–327.
6. Schneider VA, Mercola M (2001) *Genes Dev* 15:304–315.
7. Tzahor E, Lassar AB (2001) *Genes Dev* 15:255–260.
8. Wu X, Golden K, Bodmer R (1995) *Dev Biol* 169:619–628.
9. Park M, Wu X, Golden K, Axelrod JD, Bodmer R (1996) *Dev Biol* 177:104–116.
10. Naito AT, Akazawa H, Takano H, Minamino T, Nagai T, Aburatani H, Komuro I (2005) *Circ Res* 97:144–151.
11. Nakamura T, Sano M, Songyang Z, Schneider MD (2003) *Proc Natl Acad Sci USA* 100:5834–5839.
12. Keller G (2005) *Genes Dev* 19:1129–1155.
13. Ema M, Takahashi S, Rossant J (2006) *Blood* 107:111–117.
14. Hidaka K, Lee JK, Kim HS, Ihm CH, Iio A, Ogawa M, Nishikawa S, Kodama I, Morisaki T (2003) *FASEB J* 17:740–742.
15. Frasch M (1995) *Nature* 374:464–467.
16. Schultheiss TM, Burch JB, Lassar AB (1997) *Genes Dev* 11:451–462.
17. Shi Y, Katsev S, Cai C, Evans S (2000) *Dev Biol* 224:226–237.
18. Zhang H, Bradley A (1996) *Development (Cambridge, UK)* 122:2977–2986.
19. Monzen K, Shiojima I, Hiroi Y, Kudoh S, Oka T, Takimoto E, Hayashi D, Hosoda T, Habara-Ohkubo A, Nakaoka T, *et al.* (1999) *Mol Cell Biol* 19:7096–7105.
20. Huber TL, Kouskoff V, Fehling HJ, Palis J, Keller G (2004) *Nature* 432:625–630.
21. Lindsley RC, Gill JG, Kyba M, Murphy TL, Murphy KM (2006) *Development (Cambridge, UK)* 133:3787–3796.
22. Kirstetter P, Anderson K, Porse BT, Jacobsen SE, Nerlov C (2006) *Nat Immunol* 7:1048–1056.
23. Scheller M, Huelsken J, Rosenbauer F, Taketo MM, Birchmeier W, Tenen DG, Leutz A (2006) *Nat Immunol* 7:1037–1047.
24. Gupta S, Zhu H, Zon LI, Evans T (2006) *Development (Cambridge, UK)* 133:2177–2187.
25. Baker JC, Beddington RS, Harland RM (1999) *Genes Dev* 13:3149–3159.
26. Willert J, Epping M, Pollack JR, Brown PO, Nusse R (2002) *BMC Dev Biol* 2:8.
27. Winkler DG, Sutherland MS, Ojala E, Turcott E, Geoghegan JC, Shpektor D, Skonier JE, Yu C, Latham JA (2005) *J Biol Chem* 280:2498–2502.
28. Kishida S, Yamamoto H, Kikuchi A (2004) *Mol Cell Biol* 24:4487–4501.
29. Niwa H, Miyazaki J, Smith AG (2000) *Nat Genet* 24:372–376.
30. Naito AT, Tominaga A, Oyamada M, Oyamada Y, Shiraishi I, Monzen K, Komuro I, Takamatsu T (2003) *Exp Cell Res* 291:56–69.

Journal of the American College of Cardiology
© 2006 by the American College of Cardiology Foundation
Published by Elsevier Inc.

Vol. 47, No. 4, 2006
ISSN 0735-1097/06/$32.00
doi:10.1016/j.jacc.2005.09.048

Cardioprotective Effects of Granulocyte Colony-Stimulating Factor in Swine With Chronic Myocardial Ischemia

Hiroshi Hasegawa, MD, PHD, Hiroyuki Takano, MD, PHD, Koji Iwanaga, DVM, Masashi Ohtsuka, MD, PHD, Yingjie Qin, MD, Yuriko Niitsuma, MD, Kazutaka Ueda, MD, Tomohiko Toyoda, MD, PHD, Hiroyuki Tadokoro, MD, Issei Komuro, MD, PHD

Chiba, Japan

OBJECTIVES The aim of this study was to investigate the effect of granulocyte colony-stimulating factor (G-CSF) on chronic myocardial ischemia in swine.

BACKGROUND We recently have reported that G-CSF prevents cardiac remodeling and dysfunction after acute myocardial infarction in mice and swine. It remains unclear whether G-CSF has beneficial effects on chronic myocardial ischemia.

METHODS An ameroid constrictor was placed on left circumflex coronary artery of swine. The presence of myocardial ischemia was verified at four weeks after the operation, and the animals were randomly assigned into the following two groups: 1) administration of vehicle (control group, n = 10), and 2) administration of G-CSF (10 μg/kg/day) for seven days (G-CSF group, n = 10).

RESULTS Echocardiographic examination revealed that the G-CSF treatment prevented left ventricular dilation and dysfunction at eight weeks after the operation. Stress echocardiography revealed that G-CSF ameliorated the regional contractility of chronic myocardial ischemia. Morphological analysis revealed that the extent of myocardial fibrosis of the ischemic region was less in the G-CSF group than in control group. There were more vessels and less apoptotic cells at the ischemic region of the heart of the G-CSF group than control group. Moreover, Akt1 was more strongly activated in the heart of the G-CSF group than control group.

CONCLUSIONS These findings suggest that G-CSF improves cardiac function of chronic myocardial ischemia through decreases in fibrosis and apoptotic death and an increase in vascular density in the ischemic region. (J Am Coll Cardiol 2006;47:842–9) © 2006 by the American College of Cardiology Foundation

Ischemic cardiomyopathy is a leading cause of congestive heart failure in many countries (1). In chronic myocardial ischemia, contractile function is depressed because of reduced myocardial perfusion (2). The viable-but-dysfunctional myocardium could be reversed by the restoration of myocardial blood flow (3–8). Although interventional therapies such as coronary artery bypass grafting and percutaneous coronary intervention are performed to increase blood supply to ischemic region, many patients with ischemic cardiomyopathy cannot be treated because of severe and diffuse coronary atherosclerosis. The only possibility is pharmacological therapy, which reduces myocardial oxygen demand to treat chronic myocardial ischemia if interventional therapies cannot be feasible. Therefore, novel strategies in patients with severe myocardial ischemia not amenable to conventional revascularization have been awaited.

Granulocyte colony-stimulating factor (G-CSF), a hematopoietic cytokine, induces the mobilization of hematopoietic stem cells and endothelial progenitor cells (EPCs) from bone marrow into the peripheral blood circulation (9–11). Recently, several groups, including ours, have reported that G-CSF prevents left ventricular (LV) remodeling after acute myocardial infarction (MI) in mice and swine (12–17). We have demonstrated that G-CSF receptor is expressed on cardiomyocytes and that G-CSF prevents LV remodeling after MI by activating the Janus family tyrosine kinases and signal transducer and activator of transcription pathway in cardiomyocytes (17). In the present study, we examined whether G-CSF treatment is effective on chronic myocardial ischemia in swine and investigated the mechanism of beneficial effects of G-CSF.

METHODS

Swine model of chronic myocardial ischemia. Male Yorkshire swine (Science Breeding Farm, Iwate, Japan) weighing 15 to 20 kg were used to induce chronic myocardial ischemia. Ameroid-induced progressive coronary occlusion was performed as described previously (18–20). Briefly, initial sedation was achieved with intramuscularly ketamine and xylazine. An ear vein was then cannulated for administration of an infusion of ketamine and thiamylal as needed to supplemental anesthesia. The swine was intubated and ventilated with oxygen at a flow of 2 l/min and isoflurane in

From the Department of Cardiovascular Science and Medicine, Chiba University Graduate School of Medicine, Chiba, Japan. This work was supported by a Grant-in-Aid for Scientific Research, Developmental Scientific Research, and Scientific Research on Priority Areas from the Ministry of Education, Science, Sports, and Culture and by the Program for Promotion of Fundamental Studies in Health Sciences of the Organization for Drug ADR Relief, R&D Promotion and Product Review of Japan (to Dr. Komuro) and the Mochida Memorial Foundation for Medical and Pharmaceutical Research (to Dr. Takano).

Manuscript received July 14, 2005; revised manuscript received September 13, 2005, accepted September 26, 2005.

Abbreviations and Acronyms

DOB = dobutamine
ECs = endothelial cells
EPC = endothelial progenitor cell
FAC = fractional area change
G-CSF = granulocyte colony-stimulating factor
LCX = left circumflex coronary artery
LV = left ventricle
LVEDA = left ventricular end-diastolic area
LVEDP = left ventricular end-diastolic pressure
LVESA = left ventricular end-systolic area
MI = myocardial infarction
TUNEL = terminal deoxynucleotidyl transferase-mediated deoxyuridine triphosphate-digoxigenin nick end labeling
VEGF = vascular endothelial growth factor
vWF = von Willebrand factor

a concentration of 2.0%. Isoflurane was the primary anesthetic agent. After opening the chest, an ameroid constrictor (2.5 mm of internal diameter) was implanted around the proximal left circumflex coronary artery (LCX). The chronic myocardial ischemia was induced by progressive coronary artery stenosis with ameroid coronary constriction (21). All protocols were approved by the Institutional Animal Care and Use Committee of the Chiba University.

Cytokine treatment. Ameroid constrictors were implanted in 58 pigs. Twenty-three pigs died suddenly within three weeks of the implantation, possibly because of abrupt coronary occlusion or lethal arrhythmia. Four weeks after the implantation of ameroid constrictors, all surviving pigs (n = 35) underwent the following: 1) transthoracic echocardiography, 2) cardiac catheter study, and 3) selective left and right coronary artery angiography. Twenty swine of 35 that developed severe coronary stenosis and suffered from myocardial ischemia without MI were assigned randomly by an investigator (who was different from operators) into: 1) a control group (n = 10), which was injected subcutaneously with saline for seven days, or 2) G-CSF treatment group (n = 10), which was injected subcutaneously with recombinant human G-CSF (10 μg/kg/day, Kirin Brewery Co. LTD., Tokyo, Japan) for seven days. Five pigs served as sham-operated controls in which the constrictor was not implanted after opening the chest. The numbers of circulating white blood cells and granulocytes were counted before and at four and eight weeks after the operation in both groups. We also measured the serum levels of creatine kinase-MB isoenzyme and cardiac troponin I before and at one and four weeks after the operation in both groups.

Echocardiography. Echocardiographic studies were performed before surgery and at four and eight weeks after the placement of ameroid constrictors with Philips Sonos 5500 and an ultraband S4 sector transducer (Philips Medical Systems N.A., Bothell, Washington). Two-dimensional epicardial echocardiography was performed at the short-axis view at midpapillary muscle level of LV (22). Images were obtained from the epicardial surface of the right ventricle and recorded on a magnetic optical drive and video tape for offline analysis of wall thickening. Left ventricular end-diastolic area (LVEDA), left ventricular end-systolic area (LVESA), interventricular septum wall thickness in diastole, LV posterior wall thickness in diastole, and fractional area change (FAC) were measured by B-mode. The end-diastolic frame of the echocardiographic images was selected using the onset of the Q-wave of the electrocardiography; the frame with the smallest LV cavity was defined as end-systole. Regional contractility (fractional shortening) was obtained by measuring the percent wall thickening (end-systolic thickness minus end-diastolic thickness/end-diastolic thickness) of the ischemic (LCX) region ×100 (23). Stress echocardiography was performed with incremental doses of dobutamine (DOB) infusion from 5 to 40 γ at 5-min intervals. All measurements were performed at rest and under stress with 10 μg/kg/min (10 γ) and 40 μg/kg/min (40 γ) of DOB to document the presence of hibernating myocardium in LCX region. The average of three measurements in each examined region was used for analysis. The recording of echocardiography and its evaluation were performed by different persons blinded to randomization.

Cardiac catheter study. Four and eight weeks after ameroid constrictor implantation, cardiac catheter study was performed. A 6-F sheath introducer was inserted via left carotid artery and a pig-tail catheter was implanted in the LV cavity through a sheath introducer to obtain left ventricular end-diastolic pressure (LVEDP), dp/dt, and −dp/dt. Coronary angiography was performed subsequently.

Histological analysis. After the echocardiography and coronary angiography, the swine were sacrificed. After heart weight was measured, ischemic (LCX region) and nonischemic (remote region) myocardium were fixed with perfusion of 3.8% formaldehyde, embedded in paraffin for hematoxylin-eosin staining and van Gieson staining, or embedded in OCT compound for immunohistochemistry. To determine the degree of collagen fiber accumulation, we calculated the ratio of van Gieson staining fibrosis area to total myocardium area with the software NIH IMAGE 1.63 (National Institutes of Health, Bethesda, Maryland) for image analysis. The rest of myocardium was frozen and prepared for Western blot analysis. Endothelial cells (ECs) were identified immunohistochemically using anti-von Willebrand factor (vWF) antibody (Dako, Carpinteria, California) and Cy3-labeled secondary antibody. To count the numbers of vessels, 15 fields were chosen randomly from ischemic and nonischemic regions in each sample (n = 10 each group). For detection of apoptotic cells, the terminal deoxynucleotidyl transferase-mediated deoxyuridine triphosphate-digoxigenin nick end labeling (TUNEL) assay was performed using the In Situ Apoptosis Detection Kit (Takara, Japan). To identify which cells were TUNEL-positive, we performed double-staining by using anti-cardiac troponin T or anti-vWF antibody with TUNEL assay.

Western blot analysis. Whole tissue lysates were extracted from the myocardium of sham-operated swine and ischemic

Table 1. Echocardiographic Data

	Control (n = 10)			G-CSF (n = 10)		
	Pre	4 Weeks	8 Weeks	Pre	4 Weeks	8 Weeks
LVEDA (cm^2)	9.9 ± 1.5	11.1 ± 2.0	12.9 ± 2.4	9.4 ± 1.5	11.4 ± 2.4	11.1 ± 1.5*
LVESA (cm^2)	6.4 ± 1.2	7.3 ± 1.3	9.0 ± 1.7	6.2 ± 1.1	7.7 ± 1.7	7.2 ± 1.1*
FAC (%)	35.5 ± 6.0	34.1 ± 2.7	30.1 ± 4.2	34.6 ± 3.4	32.8 ± 8.0	35.1 ± 3.3*
IVSTd (mm)	5.3 ± 0.3	5.2 ± 0.3	5.2 ± 0.3	5.5 ± 0.2	5.2 ± 0.3	5.2 ± 0.3
PWTd (mm)	5.5 ± 0.2	5.0 ± 0.9	4.3 ± 0.4	5.3 ± 0.3	4.4 ± 0.4	4.4 ± 0.4

At preoperation (Pre), 4 weeks, and 8 weeks after the operation, left ventricular end-diastolic area (LVEDA), left ventricular end-systolic area (LVESA), fractional area change (FAC), interventricular septum thickness in diastole (IVSTd), and left ventricular posterior wall thickness in diastole (PWTd) at the level of midpapillary muscles in short-axis view were measured by B-mode. The average of three measurements was used for analysis. Results are given as mean ± SEM. *$p < 0.05$ vs. control group.

myocardium of operated swine and subjected to Western blot analysis. The extracts were centrifuged at 14,000 rpm at 4°C for 30 min, and the total protein concentration was measured with the BCA protein assay kit (Pierce, Illinois). Proteins (50 μg) were separated by sodium dodecyl sulfate polyacrylamide gel electrophoresis and transferred onto a nitrocellulose transfer membrane (Schleicher Schuell, the Netherlands). After blocking in TBS-T (150 mmol/l NaCl, 50 mmol/l Tris, and 0.1% Tween 20, pH 7.4) containing 5% skim milk, the membranes were incubated with antibodies against Akt1, phospho-Akt1, vascular endothelial growth factor (VEGF), or actin (Santa Cruz Biotechnology, Santa Cruz, California). Hybridizing bands were visualized using an ECL detecting kit (Amersham Pharmacia Biotech, Piscataway, New Jersey).

Statistical analysis. All data are presented as mean ± SEM. The two-tailed, unpaired Student *t* test, or one-way analysis of variance was used to compare group means, and multiple comparisons were performed using Fisher post-hoc test. A probability value of $p < 0.05$ was considered to be statistically significant. All statistical analysis was performed using StatView 4.5 software for Macintosh (SAS Institute Inc., Cary, North Carolina).

RESULTS

Swine model. At four and eight weeks after the operation, there was no difference in the body weight between two groups. All animals (n = 20) that were treated with saline or G-CSF survived throughout the study. The numbers of white blood cells and granulocytes at preoperation and one and four weeks after the operation were no different between two groups. The serum levels of creatine kinase-MB isoenzyme and cardiac troponin I at one and four weeks after the operation were within normal ranges, and no significant differences were detected between two groups (data not shown), indicating that MI was not induced by the operation. No differences were found in the serum levels of interleukin (IL)-1-beta and IL-6 before surgery or at and four and eight weeks after the operation between the two groups (data not shown).

Echocardiographic analysis. We evaluated LV function and size by echocardiography before surgery and four and eight weeks after the operation. Slight LV dilation and wall thinning with decreased contraction at the LCX region were recognized at 4 weeks after the operation (Table 1).

At eight weeks after the operation (four weeks after saline or G-CSF treatment), LV dilation became more prominent (LVEDA, 12.9 ± 2.4 cm^2; LVESA, 9.0 ± 1.7 cm^2) and LV function was worse in control group (FAC, 30.1 ± 4.2%; Table 1). Dobutamine stress echocardiography demonstrated that regional contractility of the ischemic wall showed the biphasic response to 10 γ and 40 γ of DOB at four weeks after the operation (11.1 ± 1.5% at rest; 14.5 ± 2.1% at 10 γ; 5.1 ± 1.8% at 40 γ), suggesting ischemic but viable myocardium. At eight weeks after the operation (four weeks after saline or G-CSF treatment), however, there were significant differences in the two groups. Left ventricular dilation was less in G-CSF group (LVEDA, 11.1 ± 1.5 cm^2; LVESA, 7.2 ± 1.1 cm^2) than in the control group, and LV function was better in G-CSF group (FAC, 35.1 ± 3.3%) than control group (Table 1). Furthermore, at eight weeks after the operation, regional contractility of the ischemic region at rest and under stress with DOB were significantly larger in the G-CSF group than the control group (control, 11.9 ± 2.8% vs. G-CSF 18.5 ± 2.7% at rest; control, 16.7 ± 2.3% vs. G-CSF, 23.7 ± 3.2% at 10 γ

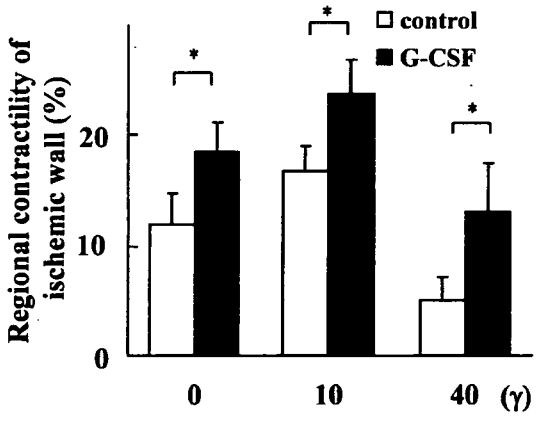

Figure 1. Regional contractility of ischemic wall. Regional contractility of ischemic (left circumflex coronary artery) wall was determined at eight weeks. Each measurement was performed without or with continuous infusion of 10 μg/kg/min (10 γ) and 40 μg/kg/min (40 γ) of dobutamine to evaluate the viable ischemic myocardium. The average of three measurements was used for analysis. Results are given as mean ± SEM (n = 10 each group). *$p < 0.05$.

Table 2. Hemodynamic Parameters by Cardiac Catheterization

	Control (n = 10)		G-CSF (n = 10)	
	4 Weeks	8 Weeks	4 Weeks	8 Weeks
dp/dt (mm Hg/s)	1,067 ± 141	1,244 ± 60	996 ± 90	1,158 ± 88
−dp/dt (mm Hg/s)	1,580 ± 179	1,871 ± 188	1,763 ± 124	1,796 ± 142
LVEDP (mm Hg)	11.2 ± 1.9	7.2 ± 2.0	9.0 ± 1.0	3.7 ± 0.7*

4 and 8 weeks after operation, cardiac catheter study was performed. dp/dt, −dp/dt, and LVEDP was measured. The average of three measurements was used for analysis. Results are given as mean ± SEM. *p < 0.05 vs. control group.

of DOB; control, 5.0 ± 2.2% vs. G-CSF, 12.9 ± 4.5% at 40 γ of DOB) (Fig. 1).

Cardiac catheter study. At four weeks after the implantation of ameroid constrictor, LCX was completely occluded and marked collateral flow was supplied from the left anterior descending artery. Blood pressure was no different between two groups at preoperation or at four weeks or eight weeks after the operation. The LVEDP, dp/dt, and −dp/dt were no different between two groups at four weeks after the operation (Table 2). At eight weeks after the operation, however, LVEDP was significantly lower in the G-CSF group than in the control group (Table 2).

Histological analysis. The heart weight to body weight ratio was significantly larger in control group than G-CSF group at four weeks after the treatment (control, 6.3 ± 0.6 g/kg vs. G-CSF, 5.6 ± 0.2 g/kg; $p < 0.05$). van Gieson staining revealed that there was less fibrosis in the heart of the G-CSF group than control group at the ischemic region (Figs. 2A to 2C). In the nonischemic region, there was no difference in fibrosis between two groups.

Because G-CSF has been reported to induce angiogenesis (24,25), we examined the number of vessels in ischemic myocardium. There were more vWF-positive vessels at the ischemic region in the G-CSF group than the control group (Figs. 3A to 3C). In nonischemic region, there was no difference in vessel numbers between two groups.

Because it is well known that apoptotic cell death contributes to progression of cardiac remodeling in post-MI heart and failing heart (26), we next measured the number of apoptotic cells in the ischemic myocardium using TUNEL assay. The number of TUNEL-positive cells in the ischemic region was smaller in the G-CSF group than the control group (control, 0.066 ± 0.006 vs. G-CSF, 0.044 ± 0.008%, $p < 0.05$) at four weeks after the treatment (Figs. 4A and 4B). Most of TUNEL-positive cells were infiltrated blood cells, and a part of TUNEL-positive cells were vascular cells (Fig. 4A).

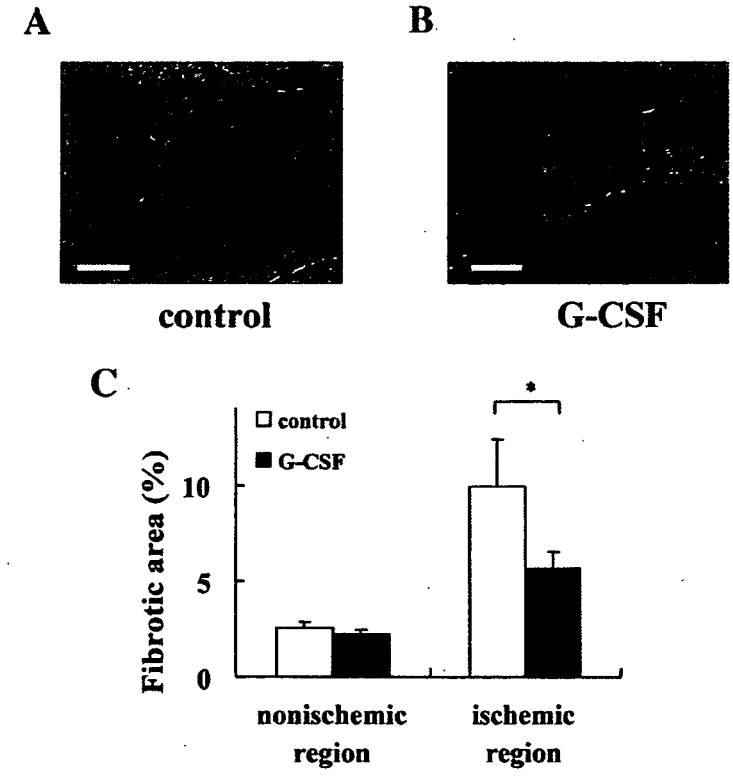

Figure 2. Fibrosis area of ischemic myocardium. Ischemic areas of control group **(A)** and granulocyte colony-stimulating factor (G-CSF)-treated group **(B)** were stained by van Gieson. Bar indicates 50 μm. **(C)** The average of fibrotic area. Results are given as mean ± SEM (n = 10 each group). *p < 0.05.

JACC Vol. 47, No. 4, 2006
February 21, 2006:842-9

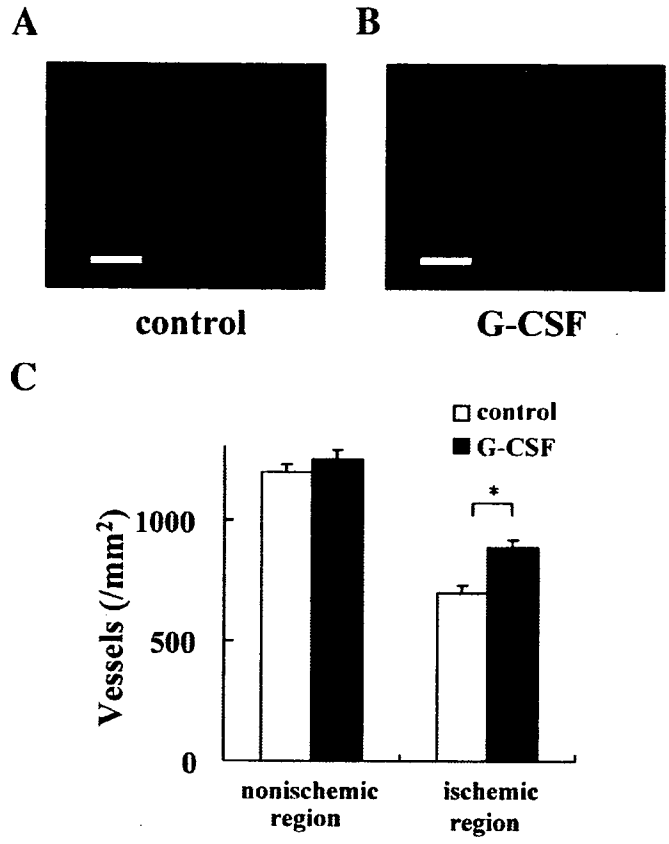

Figure 3. Number of vessels. Endothelial cells of ischemic area of control group **(A)** and granulocyte colony-stimulating factor (G-CSF)-treated group **(B)** were identified immunohistochemically using anti-von Willebrand factor antibody. Bar indicates 50 μm. **(C)** The number of vessels. Results are given as mean ± SEM (n = 10 each group). *p < 0.05.

Almost all vascular cells positive for TUNEL expressed vWF, suggesting that apoptotic cells in the vessel were ECs. The number of TUNEL-positive ECs was significantly smaller in the G-CSF treatment group (5.8 ± 1.3%) than in the control group (9.4 ± 0.7%, $p < 0.05$) (Figs. 4C and 4D). The TUNEL-positive cardiomyocytes were not detected in the ischemic region.

Activity and expression of Akt1 and VEGF. Because Akt1 has been reported to play an important role in cell survival and angiogenesis (27) and we have reported that Akt1 is activated in the infarcted heart after G-CSF treatment (16), we examined the activity of Akt1 in ischemic myocardium. Western blot analysis demonstrated that the level of phosphorylated Akt1 was lower in ischemic myocardium than in sham-operated myocardium (Figs. 5A and 5B). However, we could not demonstrate the cell types in which Akt1 was activated by G-CSF in the present study. The G-CSF treatment attenuated the down-regulation of Akt1 activity in the ischemic region (Figs. 5A and 5B). Vascular endothelial growth factor, a main member of angiogenic growth factor family, induces proliferation and survival of ECs (28). There was no significant difference in the expression level of VEGF at four weeks after the treatment between the G-CSF treatment group and the control group (Figs. 5C and 5D).

DISCUSSION

Chronic myocardial ischemia is a clinical situation that characterizes dysfunctional-but-viable myocardium as a result of an oxygen shortage due to a chronic or repetitive underperfusion accompanied by a limited coronary flow reserve (2). It has been suggested that the underperfused myocardium can retain its viability by reducing its contraction and that LV function can be recovered by restoring myocardial oxygen supply or reducing myocardial oxygen demand. Although chronic myocardial ischemia is viewed as an adaptive response to maintain cardiomyocyte viability in the setting of reduced blood flow, fibrosis is increased in ischemic myocardium (2,29,30). The beneficial effects of G-CSF on acute MI have been demonstrated, but its effects on chronic ischemic heart disease have not been determined. In the present study, we demonstrated that the G-CSF treatment also is effective on chronic myocardial ischemia. Treatment using G-CSF prevented cardiac dysfunction and remodeling after chronic ischemia induced by ameroid constrictors in a swine model. Stress echocardiography revealed that G-CSF ameliorates the regional contractility of chronic myocardial ischemia. Treatment using G-CSF decreased myocardial fibrosis and endothelial cell death in the ischemic region possibly by preventing the down-regulation of Akt1 activity.

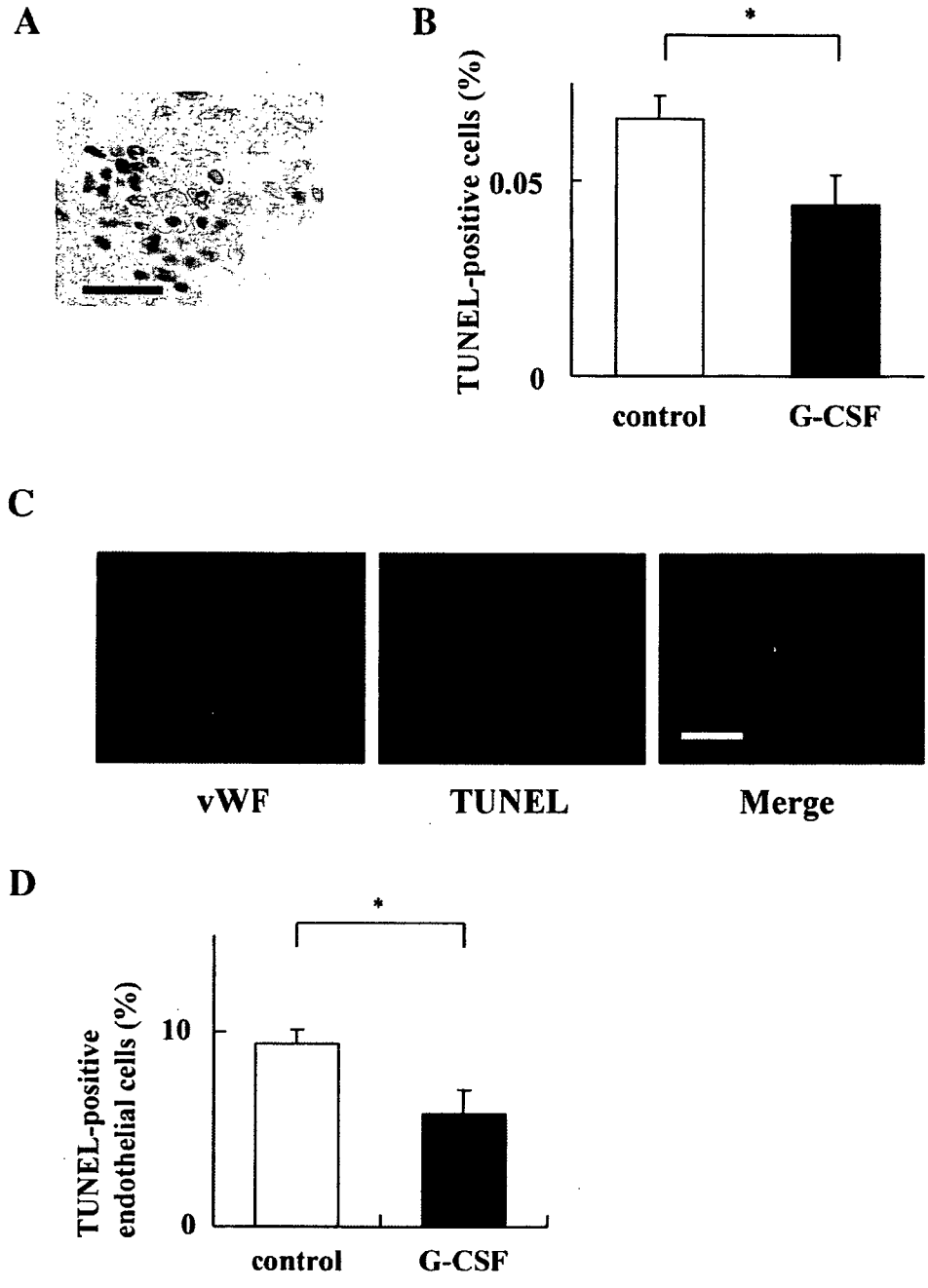

Figure 4. Apoptosis of ischemic myocardium. Apoptotic cells of ischemic area at eight weeks after the operation were identified by terminal deoxynucleotidyl transferase-mediated deoxyuridine triphosphate-digoxigenin nick end labeling (TUNEL) staining. **(A)** A representative photograph of TUNEL-positive cells. Bar indicates 30 μm. **(B)** The percentage of the number of apoptotic cells in total cells. **(C)** Representative photographs of von Willebrand factor (vWF)- and TUNEL-positive cells. Bar indicates 50 μm. **(D)** The percentage of vWF- and TUNEL-positive cells to total TUNEL-positive cells. Results are given as mean ± SEM. *$p < 0.05$.

In our echocardiographic studies at four weeks after the treatment, we found that LV function was significantly better in the G-CSF group than in the control group. Dobutamine stress echocardiography is used as a diagnostic tool to noninvasively detect coronary artery stenosis and differentiate viable from nonviable infarcted myocardium (31). Low-dose DOB improves wall thickening in the ischemic region and enhances echocardiographic detection of contractile reserve in viable ischemic myocardium, and high-dose DOB induces ischemia and deteriorates wall motion of ischemic myocardium (32). Because the biphasic response is used as a marker of both viability and inducible ischemia in the regions with viable myocardium, DOB stress echocardiography is useful to evaluate the therapeutic effects on regional contractility in chronic myocardial ischemia. The use of stress echocardiography in this study clearly demonstrated the beneficial effects of G-CSF on the ischemic region at four weeks after the treatment.

JACC Vol. 47, No. 4, 2006
February 21, 2006:842-9

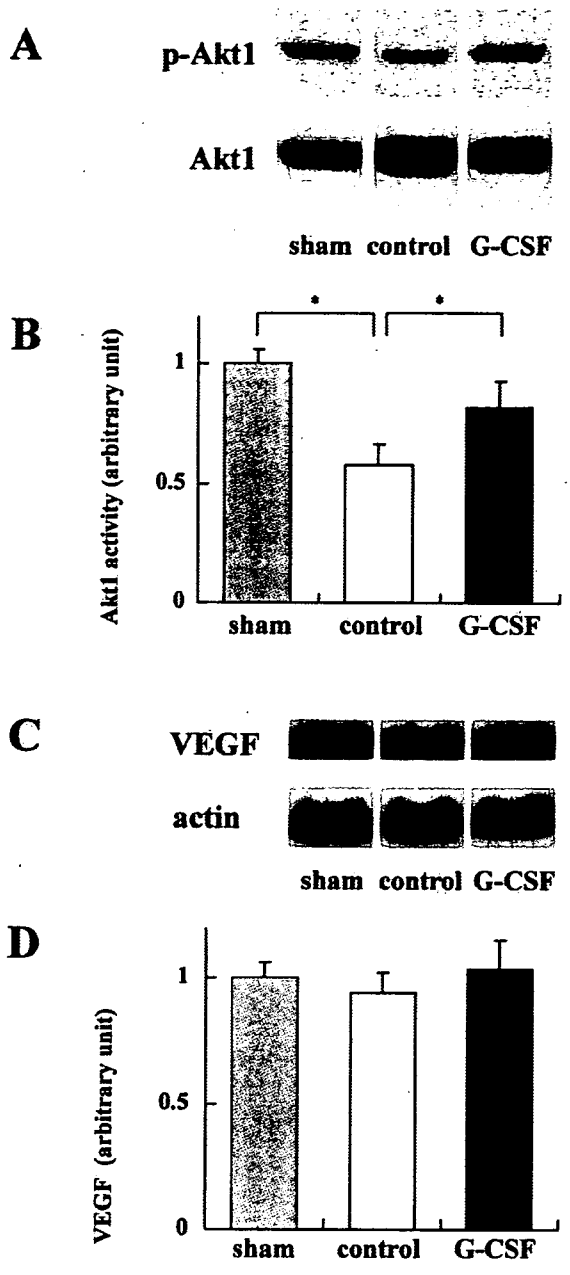

Figure 5. Akt1 activity and vascular endothelial growth factor (VEGF) expression in myocardium. Whole tissue lysates were extracted from myocardium of sham-operated swine and ischemic myocardium of operated swine, and subjected to Western blot analysis. **(A)** The membranes were incubated with antibodies against Akt1 and phospho-Akt1. Results are representative of five independent experiments. **(B)** Quantitative analysis of Akt1 activity. Results are given as mean ± SEM. **(C)** A representative photograph of VEGF expression. Results are representative of three independent experiments. **(D)** Quantitative analysis of VEGF expression. Results are given as mean ± SEM. *$p < 0.05$.

Histological analysis revealed that myocardial fibrosis was more prominent in the ischemic area compared with nonischemic area and that the treatment with G-CSF significantly reduced fibrosis. The degree of fibrosis in nonischemic area was not influenced by the treatment with G-CSF. The extent of myocardial fibrosis in the ischemic region was less in the G-CSF group than in the control group. Although it is conceivable that the decrease in death of cardiomyocytes is associated with the reduction in fibrosis, G-CSF also may modulate myocardial fibrosis through the direct effects on cardiac fibroblasts. We actually found that G-CSF receptor exists on cardiac fibroblasts (17) and that G-CSF down-regulates the expression level of collagen I in cardiac fibroblasts (Y. Qin et al, unpublished data, 2005). In the hearts after MI, the cardiac interstitium exhibits inflammatory changes, leading to increased amount of fibrosis (33). It has been reported that inflammatory cytokines such as IL-1-beta, IL-6, and tumor necrosis factor-α are involved in the generation of ischemic cardiomyopathy, including ventricular dilatation, depressed contractility, and fibrosis (34). Although there were no differences in serum levels of IL-1-beta and IL-6 before surgery and at four and eight weeks after the operation between the two groups, it remains to be determined whether expressions of inflammatory cytokines are increased in the heart.

The vessel numbers in the ischemic myocardium were larger in the G-CSF treatment group than in the control group. These results suggest that G-CSF ameliorates ischemia by increasing vessel numbers in chronic myocardial ischemia. It has been reported that the mobilization of bone marrow cells, including EPCs, are induced by G-CSF and that these cells may be involved in an increase in vessel number (9). We also observed the increase in vessel number in the heart of acute MI by treatment with G-CSF (14). Treatment using G-CSF decreased the number of apoptotic ECs in the ischemic myocardium. An increase in the vessel number, partly because of a decrease in dead ECs, may result in prevention of fibrosis and cardiac dysfunction. Although we could not detect a significant decrease in apoptotic cardiomyocytes by the G-CSF treatment, our results suggest that a G-CSF-induced increase in the vessel number may prevent cardiomyocyte death in chronically ischemic myocardium.

In ischemic myocardium, the activity of Akt1 was decreased and its activity was increased by the treatment with G-CSF. Akt1 has been reported to play a critical role in survival of cells, including ECs and cardiomyocytes (27,35). Therefore, there is a possibility that G-CSF could prevent apoptosis of cardiomyocytes even in a chronic ischemia model because G-CSF attenuated the down-regulation of Akt1 activity in the ischemic region. Because immunohistochemical analysis using anti-phospho Akt1 antibody did not work well, we could not identify in which cell types Akt1 activity was increased by G-CSF. Further studies are needed to elucidate the role of Akt1 activation induced by G-CSF in chronic myocardial ischemia. G-CSF is known to mobilize hematopoietic stem cells and EPCs into the ischemic myocardium, leading to angiogenesis. We have not examined whether G-CSF-induced mobilization of these cells plays an important role in the beneficial effects, but there is a possibility that both direct effects on myocardium and indirect effects such as mobilization and homing of stem

cells may be involved in the beneficial effects of G-CSF on chronic myocardial ischemia.

Although we have demonstrated that G-CSF has beneficial effects on chronic myocardial ischemia restricted to LCX region in the present study, G-CSF seems to have same antiapoptotic, antifibrotic, and angiogenic effects wherever the chronic ischemic region exists in myocardium. There are many patients with global ischemic cardiomyopathy in whom the culprit lesions of coronary arteries are not eligible for percutaneous coronary intervention in the clinical setting. The use of G-CSF may become a promising therapy for those patients.

Acknowledgments

The authors thank E. Fujita, R. Kobayashi, M. Ikeda, and Y. Ohtsuki for excellent technical assistance.

Reprint requests and correspondence: Dr. Issei Komuro, Department of Cardiovascular Science and Medicine, Chiba University Graduate School of Medicine, 1-8-1 Inohana, Chuo-ku, Chiba 260-8670, Japan. E-mail: komuro-tky@umin.ac.jp.

REFERENCES

1. Camici PG. Hibernation and heart failure. Heart 2004;90:141–3.
2. Heusch G, Schulz R, Rahimtoola SH. Myocardial hibernation: a delicate balance. Am J Physiol Heart Circ Physiol 2005;288:H984–99.
3. Rahimtoola SH. The hibernating myocardium. Am Heart J 1989;117: 211–21.
4. Marban E. Myocardial stunning and hibernation: the physiology behind the colloquialisms. Circulation 1991;83:681–8.
5. Ross J Jr. Myocardial perfusion-contraction matching: implications for coronary heart disease and hibernation. Circulation 1991;83: 1076–83.
6. Braunwald E, Rutherford JD. Reversible ischemic left ventricular dysfunction: evidence for the "hibernating myocardium." J Am Coll Cardiol 1986;8:1467–70.
7. Wijns W, Vatner SF, Camici PG. Hibernating myocardium. N Engl J Med 1998;339:173–81.
8. Jessup M, Brozena S. Heart failure. N Engl J Med 2003;348:2007–18.
9. Takahashi T, Kalka C, Masuda H, et al. Ischemia- and cytokine-induced mobilization of bone marrow-derived endothelial progenitor cells for neovascularization. Nat Med 1999;5:434–8.
10. Kamihata H, Matsubara H, Nishiue T, et al. Implantation of bone marrow mononuclear cells into ischemic myocardium enhances collateral perfusion and regional function via side supply of angioblasts, angiogenic ligands, and cytokines. Circulation 2001;104: 1046–52.
11. Takano H, Ohtsuka M, Akazawa H, et al. Pleiotropic effects of cytokines on acute myocardial infarction: G-CSF as a novel therapy for acute myocardial infarction. Curr Pharm Des 2003;9:1121–7.
12. Orlic D, Kajstura J, Chimenti S, et al. Mobilized bone marrow cells repair the infarcted heart, improving function and survival. Proc Natl Acad Sci USA 2001;98:10344–9.
13. Kocher AA, Schuster MD, Szabolcs MJ, et al. Neovascularization of ischemic myocardium by human bone-marrow-derived angioblasts prevents cardiomyocyte apoptosis, reduces remodeling and improves cardiac function. Nat Med 2001;7:430–6.
14. Ohtsuka M, Takano H, Zou Y, et al. Cytokine therapy prevents left ventricular remodeling and dysfunction after myocardial infarction through neovascularization. FASEB J 2004;18:851–3.
15. Minatoguchi S, Takemura G, Chen XH, et al. Acceleration of the healing process and myocardial regeneration may be important as a mechanism of improvement of cardiac function and remodeling by postinfarction granulocyte colony-stimulating factor treatment. Circulation 2004;109:2572–80.
16. Iwanaga K, Takano H, Ohtsuka M, et al. Effects of G-CSF on cardiac remodeling after acute myocardial infarction in swine. Biochem Biophys Res Commun 2004;325:1353–9.
17. Harada M, Qin Y, Takano H, et al. G-CSF prevents cardiac remodeling after myocardial infarction by activating the Jak-Stat pathway in cardiomyocytes. Nat Med 2005;11:305–11.
18. Roth DM, White FC, Nichols ML, et al. Effects of chronic exercise on regional myocardial function and coronary collateral development after gradual coronary artery occlusion in pigs. Circulation 1990;82:1778–89.
19. White FC, Carroll SM, Magnet A, Bloor CM. Coronary collateral development in swine after coronary artery occlusion. Circ Res 1992;71:1490–1500.
20. Shen YT, Vatner SF. Mechanism of impaired myocardial function during progressive coronary stenosis in conscious pigs. Hibernation versus stunning? Circ Res 1995;76:479–88.
21. Fuchs S, Kornowski R, Shiran A, Pierre A, Ellahham S, Leon MB. Electromechanical characterization of myocardial hibernation in a pig model. Coron Artery Dis 1999;10:195–8.
22. Ma L, Chen L, Gillam L, Waters DD, Chen C. Nitroglycerin enhances the ability of dobutamine stress echocardiography to detect hibernating myocardium. Circulation 1997;96:3992–4001.
23. Fuchs S, Baffour R, Zhou YF, et al. Transendocardial delivery of autologous bone marrow enhances collateral perfusion and regional function in pigs with chronic experimental myocardial ischemia. J Am Coll Cardiol 2001;37:1726–32.
24. Bussolino F, Ziche M, Wang JM, et al. In vitro and in vivo activation of endothelial cells by colony-stimulating factors. J Clin Invest 1991;87:986–95.
25. Fuste B, Mazzara R, Escolar G, Merino A, Ordinas A, Diaz-Ricart M. Granulocyte colony-stimulating factor increases expression of adhesion receptors on endothelial cells through activation of p38 MAPK. Haematologica 2004;89:578–85.
26. Abbate A, Biondi-Zoccai GGL, Baldi A. Pathophysiologic role of myocardial apoptosis in post-infarction left ventricular remodeling. J Cell Physiol 2002;193:145–53.
27. Shiojima I, Walsh K. Role of Akt signaling in vascular homeostasis and angiogenesis. Circ Res 2002;90:1243–50.
28. Zachary I. Signaling mechanisms mediating vascular protective actions of vascular endothelial growth factor. Am J Physiol Cell Physiol 2001;280:C1375–86.
29. Elsasser A, Schlepper M, Klovekorn WP, et al. Hibernating myocardium: an incomplete adaptation to ischemia. Circulation 1997;96: 2920–31.
30. Depre C, Kim SJ, John AS, et al. Program of cell survival underlying human and experimental hibernating myocardium. Circ Res 2004;95:433–40.
31. Yao SS, Chaudhry FA. Assessment of myocardial viability with dobutamine stress echocardiography in patients with ischemic left ventricular dysfunction. Echocardiography 2005;22:71–83.
32. Afridi I, Kleiman NS, Raizner AE, Zoghbi WA. Dobutamine echocardiography in myocardial hibernation. Optimal dose and accuracy in predicting recovery of ventricular function after coronary angioplasty. Circulation 1995;91:663–70.
33. Nian M, Lee P, Khaper N, Liu P. Inflammatory cytokines and postmyocardial infarction remodeling. Circ Res 2004;94:1543–53.
34. Lim H, Fallavollita JA, Hard R, Kerr CW, Canty JM Jr. Profound apoptosis-mediated regional myocyte loss and compensatory hypertrophy in pigs with hibernating myocardium. Circulation 1999;100: 2380–6.
35. Matsui T, Tao J, del Monte F, et al. Akt activation preserves cardiac function and prevents injury after transient cardiac ischemia in vivo. Circulation 2001;104:330–5.

Available online at www.sciencedirect.com
SCIENCE DIRECT
ELSEVIER
Biochemical and Biophysical Research Communications 344 (2006) 370–376
BBRC
www.elsevier.com/locate/ybbrc

G-CSF prevents the progression of atherosclerosis and neointimal formation in rabbits

Hiroshi Hasegawa [a], Hiroyuki Takano [a], Masashi Ohtsuka [a], Kazutaka Ueda [a], Yuriko Niitsuma [a], Yingjie Qin [a], Hiroyuki Tadokoro [a], Masashi Shiomi [b], Issei Komuro [a,*]

[a] *Department of Cardiovascular Science and Medicine, Chiba University Graduate School of Medicine, Chiba 260-8670, Japan*
[b] *Institute for Experimental Animals, Kobe University School of Medicine, Kobe 650-0017, Japan*

Received 3 March 2006
Available online 24 March 2006

Abstract

Granulocyte colony-stimulating factor (G-CSF) prevents left ventricular remodeling after myocardial infarction, but its effect on atherosclerosis is unknown. We examined two kinds of rabbit atherosclerosis models. Myocardial infarction-prone Watanabe heritable hyperlipidemic (WHHL-MI) rabbits were treated with G-CSF or saline for 7 days from 14 months old. The vascular injury models were created by inflating angioplasty balloon in the iliac artery of rabbits and were divided into G-CSF and saline group. G-CSF significantly reduced the stenosis score of coronary artery and lipid plaque area of thoracic aorta in WHHL-MI rabbits at 4 weeks after the treatment. In the vascular injury model, G-CSF significantly prevented an increase in neointima/media ratio at 4 weeks after the treatment. G-CSF accelerated the reendothelialization of denuded arteries, and the pretreatment with nitric oxide synthase inhibitor significantly inhibited it. These results suggest that G-CSF has a therapeutic potential for the progression of atherosclerosis.

Keywords: Atherosclerosis; Cytokine; G-CSF; Vascular injury; WHHL-MI

Granulocyte colony-stimulating factor (G-CSF) is a member of a group of glycoproteins called hematopoietic cytokines. G-CSF induces the release of hematopoietic stem cells and endothelial progenitor cells (EPCs) from bone marrow into the peripheral blood circulation. Moreover, it has been reported that G-CSF also has anti-inflammatory and anti-apoptotic effects [1]. Orlic et al. [2] have reported that pretreatment with G-CSF and stem cell factor improves cardiac dysfunction after AMI by accelerating regeneration of cardiac myocytes and vessels through mobilization of bone marrow stem cells. We and others have recently reported that G-CSF prevents left ventricular (LV) remodeling and dysfunction after acute myocardial infarction (AMI) [3–6] and chronic myocardial ischemia [7] in animal models [8]. We have demonstrated that G-CSF directly activates the Jak2/STAT3 pathway in cardiomyocytes, and has anti-apoptotic effects and angiogenic effects on post-MI hearts [6]. However, Kang et al. [9] reported that G-CSF treatment (10 μg/kg for 4 days before PCI) increased the rate of in-stent restenosis at the culprit lesion in patients with AMI or old MI who underwent elective PCI. Although the size of their clinical study was very small and the mechanism by which G-CSF accelerated restenosis was unclear, the result attracted much attention in the use of G-CSF for the patients with atherosclerosis.

There had been no suitable animal models that mimic spontaneous human coronary artery diseases. Although most MI animal models are produced by ligation of coronary artery, there is no atherosclerotic lesion in these models. In 1980, Watanabe et al. developed Watanabe heritable hyperlipidemic (WHHL) rabbits as a model for human familial hypercholeste rolemia and atherosclerosis [10–12]. Shiomi et al. [13] have developed a new WHHL strain with spontaneous MI by selective breeding of myocardial

* Corresponding author. Fax: +81 43 226 2557.
E-mail address: komuro-tky@umin.ac.jp (I. Komuro).

0006-291X/$ - see front matter © 2006 Elsevier Inc. All rights reserved.
doi:10.1016/j.bbrc.2006.03.081

infarction-prone WHHL rabbit strain and named it as the WHHL-MI rabbit. This strain has high serum levels of low-density lipoprotein (LDL)-cholesterol and shows typical coronary atheromatous plaques similar to those of human. The WHHL-MI rabbit shows the high incidence of fatal MI at ages 11–35 months [13].

Many patients with AMI are currently treated with PCI and restenosis by intimal hyperplasia is the biggest problem at present [14–16]. To use G-CSF for preventing LV remodeling after AMI, it is critical to know whether G-CSF modulates intimal hyperplasia after PCI. In the present study, we investigated the effects of G-CSF on the development of atherosclerosis using WHHL-MI rabbits and on intimal formation using the balloon injury model of rabbits.

Materials and methods

Animals. To examine the effects of G-CSF on atherosclerosis, we used two rabbit models, WHHL-MI and balloon injury model. Female WHHL-MI rabbits were bred in Institute for Experimental Animals, Kobe University School of Medicine, Kobe, Japan. We fed 1% cholesterol diet to Japanese white rabbit (purchased from Takasugi laboratory animal) for balloon injury model. All protocols were approved by the Institutional Animal Care and Use Committee of Chiba University.

G-CSF treatment and analysis in WHHL-MI rabbits. Female WHHL-MI rabbits weighing 3.0–3.5 kg were randomized into two groups. (1) G-CSF group ($n = 7$); injected subcutaneously with recombinant human G-CSF (rhG-CSF, 100 μg/kg/day, Kirin Brewery Co., Ltd., Tokyo, Japan), (2) control group ($n = 7$); injected subcutaneously with saline as the same volume as G-CSF, beginning at 14 months old and continued daily for 7 days because the coronary stenosis of WHHL-MI rabbits was significantly increased during 11–35 months of age [13].

The numbers of circulating white blood cell (WBC), red blood cell (RBC), platelet (Plt), total cholesterol (TC), triglyceride (TG), LDL-cholesterol (LDL-C), activated partial thromboplastin time (APTT), and prothrombin time (PT) were measured before and at 7 days after treatment in both animal models.

At 28 days after G-CSF treatment, WHHL-MI rabbits were sacrificed, and hearts and thoracic aorta were removed and fixed with 10% formaldehyde as reported previously [17]. Coronary atherosclerosis was examined in the right coronary artery (RCA), the left anterior descending artery (LAD), and the left circumflex artery (LCX). The coronary arteries were divided into blocks, and the blocks were embedded in paraffin. The blocks were sectioned at 1 mm intervals and 8-μm-thick cross sections from each paraffin block were cut from each ostium for 10 mm long as described previously [17].

A total of 10 sections from each block were examined. Sections of the hearts were stained with hematoxylin and eosin to analyze stenosis score. The coronary stenosis score was graded as described previously [17]. The degree of atherosclerosis was evaluated by the percent of lesion area in the surface area of intima (the surface area of lesions/the surface area of the whole intima) and by the score of stenosis in the coronary arteries [17]. The coronary stenosis score was graded as follows: no lesion, 0 points; stenosis of 10% or less narrowing, 1 point; stenosis of 10–20% narrowing, 2 points; stenosis of 20–30% narrowing, 3 points; stenosis of 30–40% narrowing, 4 points; stenosis of 40–50% narrowing, 5 points; stenosis of 50–60% narrowing, 6 points; stenosis of 60–70% narrowing, 7 points; stenosis of 70–80% narrowing, 8 points; stenosis of 80–90% narrowing, 9 points; stenosis over 90% narrowing, 10 points. These points were summed for each section, and the total points for each rabbit were also counted. To examine the cellular composition of atherosclerotic lesion, the sections were stained immunohistochemically with monoclonal antibodies against smooth muscle α-actin (1A4, Dako Cytomation) and rabbit macrophages (RAM11, Dako Cytomation), reacted with avidin–conjugated peroxidase (Dako Cytomation), and visualized with 3,3′-diaminobenzidine (Dako Cytomation). Numbers of smooth muscle cells and macrophages were counted by light microscopy and quantitatively estimated with a color image analyzer (Scion Image 1.62). Lesional components were quantitatively evaluated with the color image analyzer at a magnification of 400×, and the lesion area and the area at each lesional component were measured as described previously [11,18,19]. The descending aorta of WHHL-MI rabbit was stained with Sudan IV to calculate the atherosclerotic lesions [20]. The immunohistochemical analyses were performed in a blind fashion by two researchers.

G-CSF treatment and analysis in balloon injury model rabbits. Male Japanese white rabbits weighing 2.5–3.0 kg were used to create the iliac artery balloon injury model [15]. Rabbits were fed with 1% cholesterol diet from 2 weeks before the balloon injury to the time of sacrifice. Before angioplasty, the right common carotid artery was cannulated with 6-F sheath, and 0.014-in. guidewire was passed down the descending aorta into the common iliac artery. The bifurcation of the aorta into the common iliac arteries was used as a landmark. Noncompliant balloon angioplasty catheter (3.0/20 mm) was advanced over the guidewire into the proximal common iliac artery under fluoroscopic guidance. Each animal received 500 U of heparin intravenously before balloon inflation. The balloon injury was achieved by three inflations of each of 30-s duration to obtain a maximal balloon to artery ratio of 1.5–1. The balloon was deflated for 30 s between inflations. Rabbits were injected subcutaneously with G-CSF (G-CSF group, 100 μg/kg/day) or saline (control group) from next day of the operation for 7 days. After 1 week (each group, $n = 5$) and 4 weeks (each group, $n = 10$), rabbits were sacrificed and iliac arteries were perfused and fixed with 10% formaldehyde removed and cut into 8 μm-thickness cross sections as reported previously [15]. Sections of the artery were stained with hematoxylin and eosin to analyze the area of neointima and media. To elucidate whether G-CSF accelerates reendothelialization through mobilization of EPCs, we pretreated rabbits with a nitric oxide synthase (NOS) inhibitor, N^G-nitro-L-arginine methyl ester (L-NAME, 15 mg/kg/day), from 3 days before balloon injury to 1 week (each group, $n = 5$). To examine the cellular composition of atherosclerotic lesion, the sections were stained immunohistochemically with monoclonal antibodies against rabbit macrophage (RAM11, Dako Cytomation), CD31 (JC70A, Dako Cytomation), and neutrophil (MCA805, Serotech), reacted with avidin-conjugated peroxidase (Dako Cytomation), and visualized with 3,3′-diaminobenzidine (Dako Cytomation). The ratio of reendothelialization was calculated as the ratio of the surface covered by CD31-positive cells to the total luminal surface.

Statistical analysis. Numerical values are presented as means ± SEM. Comparisons of parameters between two groups were made with unpaired Student's t test. A probability value of $P < 0.05$ was considered to be statistically significant.

Results and discussion

Effects of G-CSF on plasma lipid content

Throughout this study, there was no AMI or death in both groups of WHHL-MI rabbits. In the WHHL-MI rabbit model, there were no significant differences in serum levels of TC, LDL-C, and TG between control group and G-CSF group (Table 1). There were also no significant differences in APTT and PT between control group and G-CSF group in both models. Although the numbers of RBC and Plt were not different, the number of WBC at 7 days after treatment was significantly higher in G-CSF group than control group (G-CSF group, $41{,}600 \pm 8450/mm^3$ vs control group, $10{,}300 \pm 1240/mm^3$, $P < 0.05$) (Table 1). The degree of increase in